Available online at www.sciencedirect.com

ScienceDirect

Geochimica et Cosmochimica Acta 172 (2016) 22–38

Geochimica et Cosmochimica Acta

www.elsevier.com/locate/gca

Combinatorial effects on clumped isotopes and their significance in biogeochemistry

Laurence Y. Yeung

Department of Earth Science, Rice University, Houston, TX 77005, USA

Received 28 May 2015; accepted in revised form 17 September 2015; Available online 30 September 2015

Abstract

The arrangement of isotopes within a collection of molecules records their physical and chemical histories. Clumped-isotope analysis interrogates these arrangements, i.e., how often rare isotopes are bound together, which in many cases can be explained by equilibrium and/or kinetic isotope fractionation. However, purely combinatorial effects, rooted in the statistics of pairing atoms in a closed system, are also relevant, and not well understood. Here, I show that combinatorial isotope effects are most important when two identical atoms are neighbors on the same molecule (e.g., O_2, N_2, and D–D clumping in CH_4). When the two halves of an atom pair are either assembled with different isotopic preferences or drawn from different reservoirs, combinatorial effects cause depletions in clumped-isotope abundance that are most likely between zero and −1‰, although they could potentially be −10‰ or larger for D–D pairs. These depletions are of similar magnitude, but of opposite sign, to low-temperature equilibrium clumped-isotope effects for many small molecules. Enzymatic isotope-pairing reactions, which can have site-specific isotopic fractionation factors and atom reservoirs, should express this class of combinatorial isotope effect, although it is not limited to biological reactions. Chemical-kinetic isotope effects, which are related to a bond-forming transition state, arise independently and express second-order combinatorial effects related to the abundance of the rare isotope. Heteronuclear moeties (e.g., C—O and C—H), are insensitive to direct combinatorial influences, but secondary combinatorial influences are evident.

In general, both combinatorial and chemical-kinetic factors are important for calculating and interpreting clumped-isotope signatures of kinetically controlled reactions. I apply this analytical framework to isotope-pairing reactions relevant to geochemical oxygen, carbon, and nitrogen cycling that may be influenced by combinatorial clumped-isotope effects. These isotopic signatures, manifest as either directly bound isotope "clumps" or as features of a molecule's isotopic anatomy, are linked to molecular mechanisms and may eventually provide additional information about biogeochemical cycling on environmentally relevant spatial scales.

1. INTRODUCTION

Studies of molecules containing more than one rare isotope indicate that isotopes are seldom distributed randomly among the isotopic variants of a molecule (Eiler, 2013). These isotope distributions in principle contain information how a molecule was formed and, to some extent, its subsequent chemical and transport history. For example, for many carbonates (Ghosh et al., 2006, 2007; Schauble et al., 2006; Dennis and Schrag, 2010; Eagle et al., 2010, 2013; Tripati et al., 2010; Dennis et al., 2011; Eiler, 2011; Thiagarajan et al., 2011; Passey and Henkes, 2012; Henkes et al., 2013; Zaarur et al., 2013; Came et al., 2014; Fernandez et al., 2014; Petrizzo et al., 2014; Tang et al., 2014; Kluge et al., 2014a, 2015; Kele et al., 2015; Kluge and John, 2015a,b), atmospheric CO_2 and O_2 (Eiler and Schauble, 2004; Affek and Eiler, 2006; Affek

E-mail address: lyeung@rice.edu

http://dx.doi.org/10.1016/j.gca.2015.09.020
0016-7037/

et al., 2007; Yeung et al., 2012, 2014; Affek, 2013; Clog et al., 2014), and CH_4 in certain environments (Stolper et al., 2014a, 2015; Wang et al., 2015), isotope-exchange reactions distribute rare isotopes at or near internal isotopic equilibrium. Under those conditions, the relative abundance of singly- and multiply-substituted isotopic versions of a molecule—its "clumped" isotope distribution—reflects isotopic equilibration temperatures. Often, however, isotope-exchange reactions are disfavored or absent, and kinetic isotope fractionation governs the distribution of isotopes within a molecular species (Affek et al., 2008, 2014; Guo et al., 2009; Yeung et al., 2009; Kluge and Affek, 2012; Saenger et al., 2012; Affek and Zaarur, 2014; Joelsson et al., 2014; Kluge et al., 2014b; Schmidt and Johnson, 2015; Wang et al., 2015). Clumping of rare isotopes in those cases likely depends in part on extrinsic factors (e.g., enzyme-substrate binding) in addition to factors intrinsic to the reaction in question (e.g., vibrational frequencies of reactants and transition states). Therefore, the range of clumped-isotope variations expected from kinetically controlled reactions, particularly those relevant to biogeochemistry, is not obvious. Rapidly improving analytical capabilities for isotope and clumped-isotope geochemistry (Young et al., 2011; Eiler et al., 2013; Ono et al., 2014) will place our understanding of these isotope effects under intense scrutiny.

Indeed, recent studies indicate that clumped-isotope geochemistry is more diverse than previously recognized. Equilibrium thermodynamic partitioning yields slight excesses in multiply-substituted species relative to a random distribution of isotopes, with the magnitude of those excesses varying with the relative zero-point energies of a molecule's isotopic variants (Wang et al., 2004; Schauble et al., 2006; Cao and Liu, 2012; Webb and Miller, 2014). However, laboratory experiments show that enzymatic reactions can produce an isotopic distribution that is depleted relative to the random distribution; biologically mediated formation of gases can lead to products with an "anticlumped" isotope distribution (Stolper et al., 2015; Wang et al., 2015; Yeung et al., 2015). The origins of these anticlumped distributions are clearly kinetic, but the prevalence and range of these signatures in nature is not yet known.

In this manuscript, I examine the systematics of the clumped-isotope distribution within simple molecules formed through kinetically controlled reactions. I analyze how isotopic preferences are propagated through elementary chemical mechanisms, and I find that the clumped-isotope distribution of products depends in part on the sampling statistics of the component atoms and not simply on bond-making chemistry. These effects, which are only evident when two atoms are combined, can dominate the product's clumped isotope distribution when other isotope effects are small. For example, when rare isotopes are paired, e.g., making ^{18}O–^{18}O or ^{15}N–^{15}N, these combinatorial effects can lead to clumped-isotope distributions that are depleted relative to the stochastic distribution of isotopes even in the absence of kinetic isotope effects during bond formation. The magnitude of these deficits depends on the isotope-pair system being studied, as well as the relative bulk isotopic composition of each atom within the isotope pair. Traditional kinetic isotope effects can yield clumped-isotope deficits or excesses in the products, but they operate in conjunction with these combinatorial effects. The influence of combinatorics is therefore likely widespread, introducing challenges to existing clumped-isotope approaches, while opening up possibilities for the application of clumped-isotope analysis to new problems in biogeochemistry.

2. THEORY

2.1. The stochastic reference frame

The clumped-isotope composition of any given isotope pair is reported relative to the stochastic distribution of isotopes, i.e.,

$$\Delta_n = \left(\frac{{}^{n}R_{sample}}{{}^{n}R_{stochastic}} - 1\right) \quad (1)$$

where R is the ratio of the multiply-substituted analyte with cardinal mass n to its most abundant isotopologue (e.g., $^{47}R = {}^{47}CO_2/{}^{44}CO_2$), with the Δ_n value reported in per mil (‰). Importantly, ${}^{n}R_{stochastic}$ is a calculated isotopologue abundance that is defined internally; it depends on the bulk isotope ratios (e.g., $^{13}C/^{12}C$) in the sample itself and not on an arbitrary external standard. This internal comparison between singly- and multiply-substituted isotopic species results in some non-intuitive clumped-isotope systematics. Mixing, for example, does not conserve Δ_n values because ${}^{n}R_{sample}$ and ${}^{n}R_{stochastic}$ do not covary linearly (Eiler and Schauble, 2004; Yeung et al., 2009; Stolper et al., 2014b; Defliese and Lohmann, 2015). At the same time, the internal comparison makes Δ_n values insensitive to reservoir effects when the only relevant process is bond alteration (Ghosh et al., 2006; Passey and Henkes, 2012; Yeung et al., 2014, 2015): in these cases, the arrangement of isotopes does not depend on the source of atoms.

This sensitivity of Δ_n values to chemistry has been investigated for isotopic equilibrium (Wang et al., 2004; Ghosh et al., 2006; Schauble et al., 2006; Cao and Liu, 2012; Hill et al., 2014; Webb and Miller, 2014) and in specific cases where kinetics are important (Eiler and Schauble, 2004; Affek et al., 2007, 2014; Guo et al., 2009; Yeung et al., 2009, 2015; Daëron et al., 2011; Kluge and Affek, 2012; Saenger et al., 2012; Joelsson et al., 2014; Stolper et al., 2015; Wang et al., 2015). Here, I approach bond formation systematically: Beginning with a conceptual model of isotope pairing by irreversible reactions, I build toward an understanding of clumped-isotope distributions in polyatomic molecules that are formed with some degree of reversibility. I focus on the systematics of bond formation, as bond scission can lead to isotopomer-dependent isotope effects that are not as easily generalized (Johnston et al., 1995; Rahn et al., 1998; Farquhar et al., 2001; Miller et al., 2005; Lyons, 2007; Ostrom et al., 2007; Chakraborty et al., 2008; Danielache et al., 2008; Hattori et al., 2011; Ono et al., 2013; Whitehill et al., 2013; Schmidt and Johnson, 2015). The simplified reaction schemes described herein have analogs in gas-phase,

biological, and geological chemistry. They provide useful starting points for predicting and interpreting natural isotopologue variations.

Throughout this manuscript I will use the term "irreversible reaction" as shorthand for all reactions in which the bond-forming step does not fractionate the isotopes that are clumped together. It is an approximation meant to simplify the conception of combinatorial clumped-isotope effects. When the atoms are directly bound together, bond formation does not fractionate isotopes only in special irreversible cases. It may be a sufficient approximation when the atom pairs being considered are not directly bound together or when the transition state for bond formation is sufficiently loose, e.g., when the rate-limiting step of a multi-step reaction is not the bond-making step of interest. The latter scenario may be most relevant to multi-step biochemical redox reactions, which can be limited by the rate of electron transfer instead of bond formation (Mathai et al., 1993).

2.2. Irreversible isotope pairing

To understand the combinatorial clumped-isotope effect qualitatively, consider, as an analog for bond-forming reactions, the act of choosing two apples from a bag. In this bag, there are apples of two colors, red and green. One chooses an apple with each hand and joins the two to make a pair. After a large number of pairs have been assembled, the color distribution of the pairs is analyzed. If neither hand had a preference for a color, then the number of red–red or green–green pairs will appear random, i.e., dictated by chance, based on the total number of apples picked. If, however, the left hand had only picked red apples while the right hand had only picked green apples, there would be no color-matched pairs, clearly fewer color-matched "clumps" than if the apples had been paired by chance alone. These two endmember cases suggest that deficits in color-matched pairs, relative to chance statistics, can also arise when the right and left hands have different color preferences. Below, I will derive this idea formally as it applies to the pairing of rare isotopes: Deficits in rare-isotope pairs, relative to the stochastic distribution of isotopes, will be apparent whenever the two halves of a symmetric dimer are assembled with unequal isotopic preferences.

2.2.1. Two-isotope systems

A simple isotope-pairing reaction to investigate is one in which two substrates are bound together by an irreversible bond-forming reaction. This class of reaction is ubiquitous in biogeochemistry and relevant to biogeochemical processes such as O_2 evolution from photosynthesis (see Section 3). The simplest form of this reaction pairs two atoms, here represented as a pair of arbitrary atoms A, through the elementary steps:

$$A + E_1 \rightleftharpoons AE_1 \quad (R1)$$

$$A + E_2 \rightleftharpoons AE_2 \quad (R2)$$

$$AE_1 + AE_2 \rightarrow A\text{–}A + E_1 + E_2 \quad (R3)$$

in which E_1 and E_2 are substrate binding sites 1 and 2, respectively. Similar reactions can be written for each isotopic substitution. The initial steps can be reversible, and are associated with an isotopic fractionation factor at each binding site. For an infinite source reservoir and a two-isotope system (i.e., A and A′, with a constant ratio of [A′]/[A]), the rate of product formation is described formally by the following differential equations:

$$\frac{d[(AA)]}{dt} = k_3[AE_1][AE_2] \quad (2)$$

$$\frac{d[(AA')]}{dt} = k_{31'}[A'E_1][AE_2] + k_{32'}[AE_1][A'E_2] \quad (3)$$

$$\frac{d[(A'A')]}{dt} = k_{3''}[A'E_1][A'E_2] \quad (4)$$

in which k_3, $k_{31'}$, $k_{32'}$, and $k_{3''}$ are the forward rates for A–A association (reaction R3), and the primes denote the number of isotopic substitutions to A′ (e.g., $k_{31'}$ is a single substitution at site 1, and $k_{32'}$ is a single substitution at site 2). The bound AE_1 and AE_2 species are described by

$$\frac{d[(AE_1)]}{dt} = k_1[A][E_1] - k_{-1}[AE_1] \quad (5)$$

$$\frac{d[(AE_2)]}{dt} = k_2[A][E_2] - k_{-2}[AE_2] \quad (6)$$

with analogous equations for reactions involving A′. In Eqs. (5) and (6), k_1 and k_{-1} represent the forward and backward rate constants, respectively, for "enzyme-substrate"-type binding (reaction R1), with the same convention describing reaction R2. At steady state for substrate binding, i.e., $d[(AE_1)]/dt = 0$ and $d[(AE_2)]/dt = 0$, etc.,

$$\frac{d[(AA)]}{dt} = k_3\left(\frac{k_1k_2}{k_{-1}k_{-2}}\right)[A]^2[E_1][E_2] \quad (7)$$

$$\frac{d[(AA')]}{dt} = \left(k_{31'}\frac{k_{1'}k_2}{k_{-1'}k_{-2}} + k_{32'}\frac{k_1k_{2'}}{k_{-1}k_{-2'}}\right)[A'][A][E_1][E_2] \quad (8)$$

$$\frac{d[(A'A')]}{dt} = k_{3''}\left(\frac{k_{1'}k_{2'}}{k_{-1'}k_{-2'}}\right)[A']^2[E_1][E_2] \quad (9)$$

The primes denote rate constants for reactions involving isotopically substituted species. When A–A bond formation has no kinetic isotope effect, i.e., $k_3 = k_{31'} = k_{32'} = k_{3''}$ (see Section 2.2.3 for discussion of the more general case), the composition of each product isotopologue is:

$${}^{A\text{–}A'}R_{sample} = \frac{[(AA')]}{[(AA)]} = \frac{[A']}{[A]}\alpha_1 + \frac{[A']}{[A]}\alpha_2 \quad (10)$$

$${}^{A'\text{–}A'}R_{sample} = \frac{[(A'A')]}{[(AA)]} = \left(\frac{[A']}{[A]}\alpha_1\right)\left(\frac{[A']}{[A]}\alpha_2\right) \quad (11)$$

where $\alpha_1 = (k_{1'}/k_{-1'})/(k_1/k_{-1})$ and $\alpha_2 = (k_{2'}/k_{-2'})/(k_2/k_{-2})$ are the isotopic fractionation factors for reactions R1 and R2, respectively. Note that the expression for ${}^{A\text{–}A'}R_{sample}$ (Eq. (10)) explicitly accounts for both A–A′ and A′–A isotopologues. The stochastic distribution of isotopes in the product is thus:

$${}^{A'\text{–}A'}R_{stochastic} = \left(\frac{[A']_{product}}{[A]_{product}}\right)^2 = \left\{\frac{[(AA')] + 2[(A'A')]}{2[(AA)] + [(AA')]}\right\}^2 = \left\{\frac{{}^{A\text{–}A'}R_{sample} + 2^{A'\text{–}A'}R_{sample}}{2 + {}^{A\text{–}A'}R_{sample}}\right\}^2 \quad (12)$$

and the clumped-isotope composition of the products is therefore

$$\Delta_{A'-A'} = \left[\frac{\alpha_1\alpha_2\{2+\frac{[A']}{[A]}(\alpha_1+\alpha_2)\}^2}{\{\alpha_1+\alpha_2+2\frac{[A']}{[A]}\alpha_1\alpha_2\}^2} - 1\right] \quad (13)$$

This exact expression reveals a dependence of $\Delta_{A'-A'}$ on the fractionation factors in reactions R1 and R2 (i.e., α_1 and α_2, respectively) as well as the rare-isotope abundance of the source reservoir (i.e., [A′]/[A]). The clumped-isotope distribution of the A–A pair therefore depends on two factors that are unrelated to A–A bond-forming chemistry. The consequences of these combinatorial systematics are plotted in Fig. 1 for several isotope pairs; in general, they lead to products with fewer rare-isotope pairs than a stochastic distribution would predict.

To understand the origin of these nonstochastic clumped-isotope deficits, it is useful to examine equation (13) in the low-abundance limit, i.e., [A′]/[A] → 0. In that limit, the clumped-isotope composition can be approximated as:

$$\Delta_{A'-A'} \approx \left[\frac{\alpha_1\alpha_2}{\frac{1}{4}(\alpha_1+\alpha_2)^2} - 1\right] = \left[\frac{(\alpha_1\alpha_2)^{\frac{1}{2}}}{\frac{1}{2}(\alpha_1+\alpha_2)}\right]^2 - 1 \quad (14)$$

The combinatorial effect for isotope pairing is thus fundamentally related to the ratio of the geometric mean, $(\alpha_1\alpha_2)^{1/2}$, and the arithmetic mean, $\frac{1}{2}(\alpha_1+\alpha_2)$, of the bound species' isotopic composition. The geometric mean characterizes the number of doubly-substituted (isotopically clumped) isotopologues, while the arithmetic mean characterizes the number of singly-substituted isotopologues. Because the geometric mean of two numbers is always equal to or less than their arithmetic mean, purely combinatorial isotope effects almost always yield an "anticlumped" isotope distribution (i.e., $\Delta_{A'-A'} \leqslant 0$ with a couple exceptions; see Fig. 1 and discussion below). One can also consider this phenomenon as symmetry-based: When the two halves of a symmetric dimer are assembled through reactions R1, R2, R3, the abundances of singly-substituted product isotopomers may not be equal (i.e., [A′–A] ≠ [A–A′]). Yet, the arithmetic mean of the isotopomer abundances is still nearly equal to the bulk isotopic composition of A′ (for systems in which [A′]/[A] → 0). The geometric mean of the isotopomer abundances, however, will be smaller than the arithmetic mean, resulting in $\Delta_{A'-A'} < 0$. In contrast, for a symmetric mechanism that produces [A′–A] and [A–A′] in equal abundance (i.e., $\alpha_1 = \alpha_2$), the arithmetic and geometric means of isotopomer abundances are equal, yielding $\Delta_{A'-A'} \approx 0$.

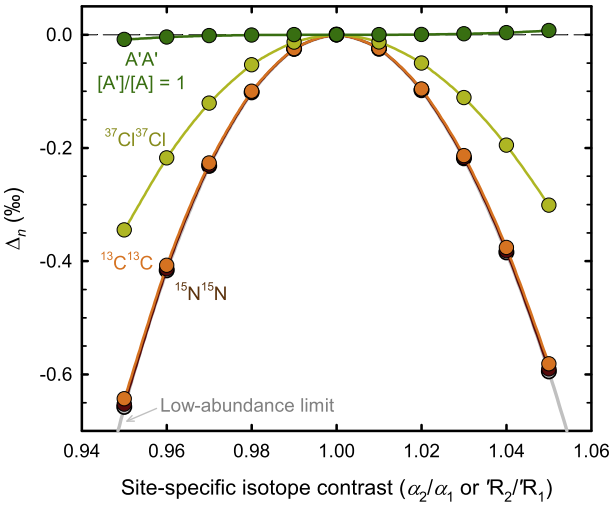

Fig. 1. Calculated clumped-isotope signatures for irreversible isotope-pairing reactions R1, R2, and R3 for $\alpha_1 = 1$. Combinatorial effects, driven here by a difference in isotopic fractionation for the two halves of a symmetric dimer, cause Δ_n values to be less than zero. As the isotopic contrast deviates from unity (plotted here as $\alpha_2/\alpha_1 = 1$ for no isotopic contrast), the magnitude of the combinatorial effect increases quadratically. The sensitivity of Δ_n values to site-specific isotope contrast decreases as rare-isotope abundance increases ($^{15}N \rightarrow {}^{13}C \rightarrow {}^{37}Cl$ at natural abundances covers two orders of magnitude).

Many isotopologue systems, such as those for H_2 and N_2, are close to the low-abundance limit described by Eq. (14) (see Fig. 1). For example, when $\alpha_1 = 1$ and $\alpha_2 = 1.05$, $\Delta_{A'-A'} = -0.59‰$ in the low-abundance limit, and the deviation from that is +0.0002‰ for D–D pairing and + 0.01‰ for a ^{13}C–^{13}C pairing. Species with more abundant rare isotopes have larger nominal departures from the low-abundance limit, such as +0.3‰ for ^{37}Cl–^{37}Cl and +0.59‰ for ^{81}Br–^{81}Br. In the endmember case in which [A′]/[A] = 1, the isotopes in the product are in slight excess relative to the stochastic distribution ($\Delta_{A'-A'} = +0.007‰$, or +0.6‰ relative to that expected in the low-abundance limit). This excess arises from the [A′]/[A]-dependent terms in Eq. (13), and is likely near the upper limit for $\Delta_{A'-A'}$ values caused by biological enzyme-substrate binding. For isotopic fractionation factors $\alpha = 0.95 - 1.05$, $\Delta_{A'-A'}$ values do not exceed 0.01‰ when [A′]/[A] = 1. Another consequence of the [A′]/[A]-dependent terms in Eq. (13) is a slight asymmetry in for $\Delta_{A'-A'}$ values $\alpha < 1$ vs. $\alpha > 1$.

In principle, $\Delta_{A'-A'}$ also depends on the isotopic composition of the source reservoir. However, the dependence of $\Delta_{A'-A'}$ on isotopic composition is generally negligible if the molecule is built from a single source of constant isotopic composition. For example, hydrogen isotope pairing from an infinite source with an extreme δD_{SMOW} value of +500‰ (SMOW = Standard Mean Ocean Water) produces Δ_4 that is only 0.0001‰ (0.1 ppm) higher than from a source with $\delta D_{SMOW} = 0$. Similarly, chlorine isotope pairing from a source with high $\delta^{37}Cl_{SMOC} = +10‰$ (SMOC = Standard Mean Ocean Chloride) produces Δ_{74} that is 0.002‰ higher than from a source with $\delta^{37}Cl_{SMOC} = 0$. If each atom is drawn from a different reservoir, however (e.g., $\delta D_{SMOW} = +500‰$ at one site and $\delta D_{SMOW} = 0$ at the second), then the characteristic dependence of Δ_n values on binding fractionation factors is offset; an "anticlumped" isotope distribution could be produced even when $\alpha_1 = \alpha_2$, and a stochastic distribution could be produced when $\alpha_1 \neq \alpha_2$. In those cases, the generalized expression for $\Delta_{A'-A'}$ produced, in terms of site-specific isotope ratios $'R_1 = \alpha_1[A']/[A]$ and $'R_2 = \alpha_2[A']/[A]$, is calculated from Eq. (13) to be:

$$\Delta_{A'-A'} = \left[\frac{{}'R_1{}'R_2(2+{}'R_1+{}'R_2)^2}{({}'R_1+{}'R_2+2{}'R_1{}'R_2)^2}-1\right] \quad (15)$$

A contrast in isotopic abundances at each site, irrespective of its origin, will lead to a nonstochastic deficit in rare-isotope pairs in the product molecules. Note, however, that Eqs. (13) and (15) describe instantaneous $\Delta_{A'-A'}$ values, i.e., the $\Delta_{A'-A'}$ values for a given set of conditions. Changing ${}'R_1$ and ${}'R_2$ values, e.g., in systems with finite atom reservoirs subject to Rayleigh fractionation, could result in instantaneous Δ_n values that vary over time.

Finally, the sensitivity of $\Delta_{A'-A'}$ values to bulk isotopic composition increases with the abundance of the rare-isotope pair. Concomitantly, however, the sensitivity of $\Delta_{A'-A'}$ values to α_1 and α_2 values decreases (Fig. 1). In this sense, stable-isotope systems with a rare minor isotope have larger combinatorial effects, all else equal. Isotope-labeling experiments, for which combinatorial clumped-isotope effects will be less important, may allow one to disentangle intrinsic kinetic isotope effects from combinatorial effects on the clumped-isotope distributions observed in natural systems.

2.2.2. Three-isotope systems

To describe species that contain three isotopes, e.g., ^{16}O, ^{17}O, and ^{18}O, I introduce the isotope A^*, which can pair with A and A′ to form the A–A^*, A^*–A^*, and A^*–A′ isotopologues with abundances described by

$${}^{A-A^*}R_{sample} = \frac{[(AA^*)]}{[(AA)]} = \frac{[A^*]}{[A]}\alpha_{1^*} + \frac{[A^*]}{[A]}\alpha_{2^*} \quad (16)$$

$${}^{A^*-A^*}R_{sample} = \frac{[(A^*A^*)]}{[(AA)]} = \left(\frac{[A^*]}{[A]}\alpha_{1^*}\right)\left(\frac{[A^*]}{[A]}\alpha_{2^*}\right) \quad (17)$$

$${}^{A^*-A'}R_{sample} = \frac{[(A^*A')]}{[(AA)]} = \left(\frac{[A^*]}{[A]}\alpha_{1^*}\right)\left(\frac{[A']}{[A]}\alpha_{2}\right) + \left(\frac{[A']}{[A]}\alpha_{1}\right)\left(\frac{[A^*]}{[A]}\alpha_{2^*}\right) \quad (18)$$

The stochastic distribution of A′ in A′–A′ becomes:

$${}^{A'-A'}R_{stochastic} = \left\{\frac{{}^{A-A'}R_{sample} + {}^{A^*-A'}R_{sample} + 2^{A'-A'}R_{sample}}{2+{}^{A-A'}R_{sample}+{}^{A-A^*}R_{sample}}\right\}^2 \quad (19)$$

which yields

$$\Delta_{A'-A'} = \left[\frac{\alpha_1\alpha_2\left\{2+\frac{[A^*]}{[A]}(\alpha_{1^*}+\alpha_{2^*})+\frac{[A']}{[A]}(\alpha_1+\alpha_2)\right\}^2}{\left\{\alpha_1+\alpha_2+2\frac{[A']}{[A]}\alpha_2\alpha_1+\frac{[A^*]}{[A]}(\alpha_{1^*}\alpha_2+\alpha_1\alpha_{2^*})\right\}^2}-1\right] \quad (20)$$

for a common and infinite reservoir, and

$$\Delta_{A'-A'} = \left[\frac{{}'R_1{}'R_2(2+{}^*R_1+{}^*R_2+{}'R_1+{}'R_2)^2}{({}'R_1+{}'R_2+2{}'R_1{}'R_2+{}^*R_1{}'R_2+{}'R_1{}^*R_2)^2}-1\right] \quad (21)$$

when generalized to the individual isotope ratios at each site. Similar expressions can be derived for $\Delta_{A^*-A^*}$. Eqs. (20) and (21) resemble Eqs. (13) and (15), except with additional terms involving the third isotope. These terms represent the sequestration of A and A′ in molecular bonds with A^*, which affects the stochastic distribution of isotopes. In molecular oxygen, this sequestration leads to negligible effects on the clumped-isotope distribution: Ignoring the contribution from ^{17}O when calculating Δ_{36} for ^{18}O–^{18}O isotope pairing only results in an error of −0.0003‰ when $\alpha_1 = 1$ and $\alpha_2 = 1.05$.

The presence of a third isotope also allows for the formation of a third clumped-isotope composition, $\Delta_{A^*-A'}$. The stochastic abundance for A^*–A′ is defined as:

$$\begin{aligned}{}^{A^*-A'}R_{stochastic} &= 2\left(\frac{[A^*]_{product}}{[A]_{product}}\right)\left(\frac{[A']_{product}}{[A]_{product}}\right)\\ &= 2\left\{\frac{[(AA^*)]+[(A^*A')]+2[(A^*A^*)]}{2[(AA)]+[(AA')]+[(AA^*)]}\right\}\\ &\quad\times\left\{\frac{[(AA')]+[(A^*A')]+2[(A'A')]}{2[(AA)]+[(AA')]+[(AA^*)]}\right\}\\ &= 2\left\{\frac{{}^{A-A^*}R_{sample}+{}^{A^*-A'}R_{sample}+2^{A^*-A^*}R_{sample}}{2+{}^{A-A'}R_{sample}+{}^{A-A^*}R_{sample}}\right\}\\ &\quad\times\left\{\frac{{}^{A-A'}R_{sample}+{}^{A^*-A'}R_{sample}+2^{A'-A'}R_{sample}}{2+{}^{A-A'}R_{sample}+{}^{A-A^*}R_{sample}}\right\}\end{aligned} \quad (22)$$

making the clumped-isotope distribution:

$$\Delta_{A^*-A'} = \left[\frac{(\alpha_{1^*}\alpha_2+\alpha_1\alpha_{2^*})\left[2+\frac{[A^*]}{[A]}(\alpha_{1^*}+\alpha_{2^*})+\frac{[A']}{[A]}(\alpha_1+\alpha_2)\right]^2}{2\left[2\frac{[A']}{[A]}\alpha_1\alpha_2+\frac{[A^*]}{[A]}(\alpha_{1^*}\alpha_2+\alpha_{2^*}\alpha_1)+\alpha_1+\alpha_2\right]\left[2\frac{[A^*]}{[A]}\alpha_{1^*}\alpha_{2^*}+\frac{[A']}{[A]}(\alpha_{1^*}\alpha_2+\alpha_1\alpha_{2^*})+\alpha_{1^*}+\alpha_{2^*}\right]}-1\right] \quad (23)$$

$$= \left[\frac{({}^*R_1{}'R_2+{}'R_1{}^*R_2)(2+{}^*R_1+{}^*R_2+{}'R_1+{}'R_2)^2}{2({}^*R_1+{}^*R_2+{}^*R_1{}'R_2+{}'R_1{}^*R_2+2{}^*R_1{}^*R_2)({}'R_1+{}^R{}_2+{}^*R_1{}'R_2+{}'R_1{}^*R_2+2{}'R_1{}'R_2)}-1\right] \quad (24)$$

In the low-abundance limit, expression (23) simplifies to

$$\Delta_{A^*-A'} \approx \left[\frac{\alpha_{1^*}\alpha_2+\alpha_1\alpha_{2^*}}{\frac{1}{2}(\alpha_1+\alpha_2)(\alpha_{1^*}+\alpha_{2^*})}-1\right] \quad (25)$$

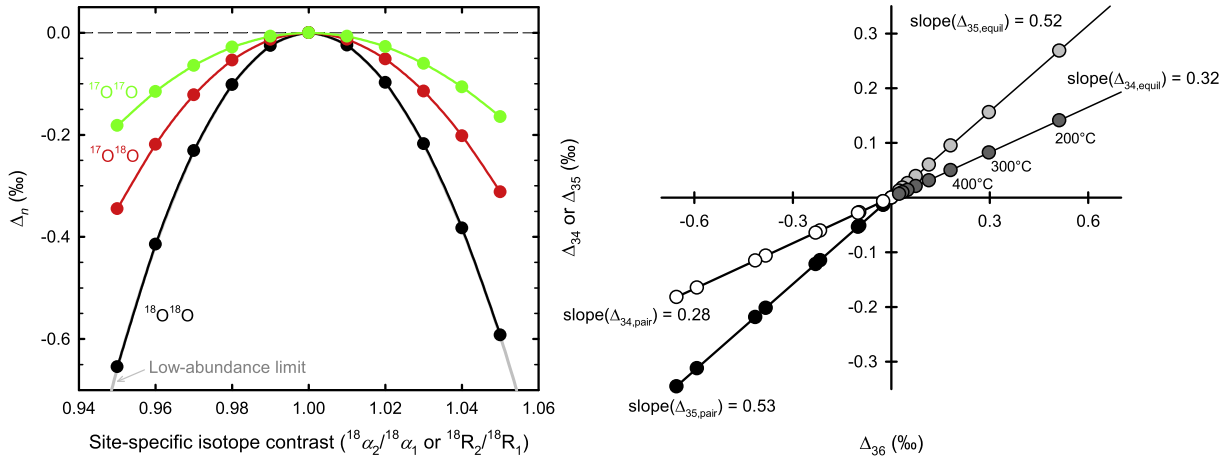

Fig. 2. Calculated combinatorial effects for rare-isotope pairing in O_2. (Left) Dependence of Δ_{34} ($^{17}O^{17}O$), Δ_{35} ($^{17}O^{18}O$), and Δ_{36} ($^{18}O^{18}O$) on site-specific isotope contrast, where the mass-dependent relationship $^{17}R = (^{18}R)^{0.528}$ was used. The smaller fractionation of ^{17}O vs. ^{18}O at each binding site results in Δ_{34} and Δ_{35} values being less sensitive to $^{18}R_2/^{18}R_1$ compared to Δ_{36}. (Right) Covariation in Δ_{34}, Δ_{35}, and Δ_{36} values for combinatorial isotope pairing (black and white points) and isotopic equilibrium (grey points). Combinatorial effects result in clumped-isotope compositions in quadrant III, while isotopic equilibrium yields clumped-isotope compositions in quadrant I. The slopes of the trends in Δ–Δ space are also unique to each process within each quadrant.

Combinatorial effects for isotope pairing in the oxygen system are shown in Fig. 2. Qualitatively, they resemble those in Fig. 1: nonstochastic deficits in rare-isotope pairs are expected, and they increase in magnitude as the two sites' isotopic preferences diverge. However, mass-dependent relationships between the three multiply-substituted isotopologues are apparent in Δ_{36}–Δ_{34} and Δ_{36}–Δ_{35} plots. They correspond to mass-dependent relationships between ^{16}O, ^{17}O and ^{18}O.

The expression for combinatorial effects on Δ_n increases in complexity as the number of relevant isotopes increases. Yet, the qualitative dependence of Δ_n on fractionation factors remains the same: Combinatorial factors almost always drive Δ_n values toward "anticlumped" values less than zero for irreversible isotope-pairing processes.

2.2.3. Isotope pairing controlled by the A–A transition state

Consider the case when two atoms from the same infinite reservoir (A or A′) are joined through a transition state to make a diatomic molecule (A–A):

$$AE_1 + AE_2 \rightleftharpoons (E_1A\text{–}AE_2)^{\ddagger} \rightarrow A\text{–}A + E_1 + E_2 \qquad (R4)$$

In classical transition state theory (Eyring, 1935; Bigeleisen and Wolfsberg, 1958), the abundance of A–A products depends on (1) the reversible association of reactants AE_1 and AE_2 that forms the transition state $(E_1A\text{–}AE_2)^{\ddagger}$ and (2) the rate of A–A formation from that transition state. This schematic example is analogous to the case in which an isotopomer-specific fractionation exists during A–A isotope pairing (i.e., $k_3 \neq k_{31'} \neq k_{32'} \neq k_{3''}$ in Eqs. 2–4).

Let k_3 and k_{-3} represent the forward and backward rate constants, respectively, for the association of the transition state, and let k_4 represent the rate constant (i.e., transmission coefficient) for A–A production from that transition state. The relevant reaction rate expressions are:

$$\frac{d[(AA)]}{dt} = k_4[(E_1A\text{–}AE_2)^{\ddagger}] \qquad (26)$$

$$\frac{d[(E_1A\text{–}AE_2)^{\ddagger}]}{dt} = k_3[AE_1][AE_2] - k_{-3}[(E_1A\text{–}AE_2)^{\ddagger}] \qquad (27)$$

If the reaction is in steady state with respect to $(E_1A\text{–}AE_2)^{\ddagger}$, i.e., $d[(E_1A\text{–}AE_2)^{\ddagger}]/dt = 0$, then

$$\frac{d[(AA)]}{dt} = \frac{k_3k_4}{k_{-3}}\left(\frac{k_1k_2}{k_{-1}k_{-2}}\right)[A]^2[E_1][E_2] \qquad (28)$$

with similar expressions for the production of the singly- and doubly-substituted isotopologues of the product:

$$\frac{d[(AA')]}{dt} = \left[\left(\frac{k_{31'}k_{41'}}{k_{-31'}}\right)\left(\frac{k_{1'}k_2}{k_{-1'}k_{-2}}\right) + \left(\frac{k_{32'}k_{42'}}{k_{-32'}}\right)\left(\frac{k_1k_{2'}}{k_{-1}k_{-2'}}\right)\right] \times [A'][A][E_1][E_2] \qquad (29)$$

$$\frac{d[(A'A')]}{dt} = \frac{k_{3''}k_{4''}}{k_{-3''}}\left(\frac{k_{1'}k_{2'}}{k_{-1'}k_{-2'}}\right)[A']^2[E_1][E_2] \qquad (30)$$

Integrating with respect to time and assuming that the source of A and A′ is infinite, the isotopologue ratios are:

$$^{A\text{–}A'}R_{sample} = \frac{[(AA')]}{[(AA)]} = \left(\frac{[A']}{[A]}\right)(\alpha_1\alpha_{k1'} + \alpha_2\alpha_{k2'}) \qquad (31)$$

$$^{A'\text{–}A'}R_{sample} = \frac{[(A'A')]}{[(AA)]} = \alpha_{k''}\left(\frac{[A']}{[A]}\right)^2\alpha_1\alpha_2 \qquad (32)$$

in which $\alpha_{k1'} = (k_{31'}k_{41'}/k_{-31'})/(k_3k_4/k_{-3})$, $\alpha_{k2'} = (k_{32'}k_{42'}/k_{-32'})/(k_3k_4/k_{-3})$, and $\alpha_{k''} = (k_{3''}k_{4''}/k_{-3''})/(k_3k_4/k_{-3})$ are the kinetic fractionation factors for reaction R4. Isotopomer-dependent transmission factors, e.g., $k_{4''}$, are uncommon because of the nearly identical potential energy surfaces for isotopically substituted reactions (Bigeleisen and Wolfsberg, 1958); they are included here for completeness. The clumped-isotope composition of the product is therefore

$$\Delta_{A'-A'} = \left[\frac{\alpha_1\alpha_2\alpha_{k''}\left\{2+\frac{[A']}{[A]}(\alpha_1\alpha_{k1'}+\alpha_2\alpha_{k2'})\right\}^2}{\left\{\alpha_1\alpha_{k1'}+\alpha_2\alpha_{k2'}+2\frac{[A']}{[A]}\alpha_1\alpha_2\alpha_{k''}\right\}^2}-1\right] \quad (33)$$

$$= \left[\frac{{}'R_1{}'R_2\alpha_{k''}(2+{}'R_1\alpha_{k1'}+{}'R_2\alpha_{k2'})^2}{({}'R_1\alpha_{k1'}+{}'R_2\alpha_{k2'}+2{}'R_1{}'R_2\alpha_{k''})^2}-1\right] \quad (34)$$

which are generalizations of Eqs. (13) and (15).

While the dependence of $\Delta_{A'-A'}$ on kinetic fractionation factors is not straightforward, the basic form of Eqs. (33) and (34) can be understood more clearly when $\alpha_{k'} = \alpha_{k1'} = \alpha_{k2'}$, i.e.:

$$\Delta_{A'-A'} \approx \left[\frac{\alpha_1\alpha_2\left\{2+\frac{[A']}{[A]}(\alpha_1+\alpha_2)\alpha_{k'}\right\}^2}{\left\{\alpha_1+\alpha_2+2\left(\frac{\alpha_{k''}}{\alpha_{k'}}\right)\frac{[A']}{[A]}\alpha_1\alpha_2\right\}^2}\times\frac{\alpha_{k''}}{(\alpha_{k'})^2}-1\right] \quad (35)$$

and the rare-isotope abundance is vanishingly low (i.e., $[A']/[A] \to 0$):

$$\Delta_{A'-A'} \approx \left[\frac{\alpha_1\alpha_2}{\frac{1}{4}(\alpha_1+\alpha_2)^2}\times\frac{\alpha_{k''}}{(\alpha_{k'})^2}-1\right] \quad (36)$$

Similar expressions can be derived for triple-isotope systems. The first term in Eqs. (35) and (36) is the pure combinatorial effect, analogous to the first term in Eqs. (13) and (14), respectively. The second term, determined by the physical chemistry of the $(E_1A–AE_2)^‡$ transition state, is the chemical preference for rare-isotope clumping in excess of the stochastic distribution. It can be extracted from quantum–mechanical calculations of transition-state properties (Guo et al., 2009; Joelsson et al., 2014).

When $\alpha_{k''}/(\alpha_{k'})^2 > 1$, kinetic isotope fractionation leads directly to $\Delta_{A'-A'} > 0$, while if $\alpha_{k''}/(\alpha_{k'})^2 < 1$, it leads to $\Delta_{A'-A'} < 0$. As illustrated in Fig. 3, the $\Delta_{A'-A'}$ value has a first-order dependence on $\alpha_{k''}$ and a second-order (or weaker) dependence on the other isotopic fractionation factors. The magnitude of kinetic isotope effects (i.e., the tightness of the transition state) controls the importance of combinatorial effects in reactions like R4.

When kinetic isotope effects are small [i.e., $\alpha_{k''}/(\alpha_{k'})^2 \to 1$], $\Delta_{A'-A'}$ values are dominated by combinatorial "anti-clumping," likely of order 0–−1‰. Even when kinetic isotope effects are large [i.e., $\alpha_{k''}/(\alpha_{k'})^2 \neq 1$], combinatorial effects tend to reduce the effective preference for rare-isotope pairs; they generally decrease $\Delta_{A'-A'}$ values (see Fig. 3). For example, a transition state that pairs ^{18}O atoms by 5‰ moreso than what chance dictates, i.e., $\alpha_{k''}/(\alpha_{k'})^2 = 1.005$, will express a $\Delta_{18O-18O}$ value in its products that is slightly less than 5‰. An asymmetry in substrate-binding fractionation reduces the $\Delta_{18O-18O}$ value further: For $^{18}\alpha_2/^{18}\alpha_1$ values between 0.95 and 1.05, combinatorial effects reduce the product's $\Delta_{18O-18O}$ values to between 4.32‰ and 4.98‰. If, instead, $\alpha_{k''}/(\alpha_{k'})^2 = 0.995$ for the transition state, then $\Delta_{18O-18O}$ values would be between −5.63‰ and −4.98‰ instead of −5.00‰ in the absence of combinatorial effects. Furthermore, increasing rare-isotope abundance decreases the sensitivity of $\Delta_{A'-A'}$ values to chemical-kinetic effects, rendering combinatorial effects more important (see Fig. 3). However, rare-isotope abundance, i.e., $[A']/[A]$, can modulate the magnitude of the combinatorial term in Eq. (35). Similar to the case for irreversible reactions (Section 2.2.1), $\Delta_{A'-A'}$ values here become less sensitive to site-specific isotope contrast as $[A']/[A]$ increases. For example, when when $\alpha_{k''}/(\alpha_{k'})^2 = 1.005$, pairing of ^{18}O atoms at natural abundances results in a maximum $\Delta_{18O-18O}$ value of 4.98‰, which is reduced to 4.38‰ (i.e., −0.60‰) when $^{18}\alpha_2/^{18}\alpha_1 = 1.05$; a hypothetical transition state that pairs ^{37}Cl atoms, which have a relative abundance ~100 times higher, has a maximum $\Delta_{37Cl-37Cl}$ value of 2.57‰, which is only reduced to 2.22‰ (i.e., −0.35‰) when $^{37}\alpha_2/^{37}\alpha_1 = 1.05$.

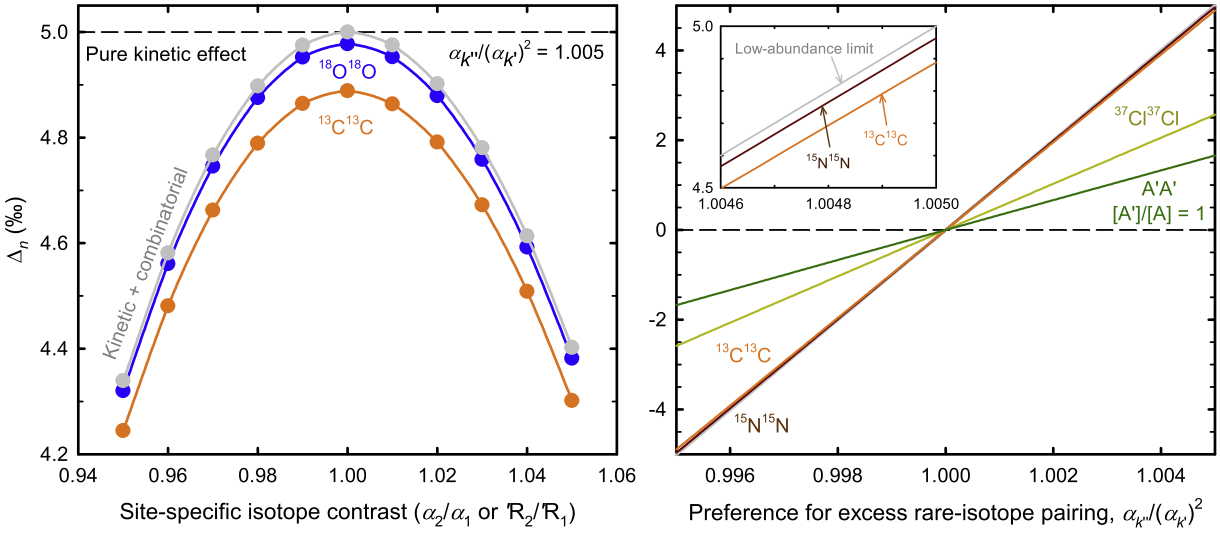

Fig. 3. Calculated combinatorial effects for reversible (but kinetically controlled) rare-isotope pairing. (Left) Rare-isotope paring is strongly dependent on intrinsic kinetic clumping/anticlumping preferences, i.e., $\alpha_{k''}/(\alpha_{k'})^2$ in Eq. (35), but depletions in Δ_n values caused by combinatorial effects are still relevant. (Left and right) Increasing abundance of the rare isotope reduces the sensitivity of Δ_n values to clumping/anticlumping preferences; $^{15}N \to {}^{13}C \to {}^{37}Cl$ at natural abundances covers two orders of magnitude. This secondary combinatorial effect arises from the $[A']/[A]$-dependent terms in Eqs. 33–35.

Eqs. 33–35 also apply to reactions in which the first substrate is bound and the second reacts directly by making an A–A bond, i.e.,

$$AE_1 + A \rightleftharpoons (E_1A\text{–}A)^{\ddagger} \rightarrow A\text{–}A + E_1 \quad (R5)$$

This reaction mechanism applies to a variety of processes such as denitrification [(Riplinger and Neese, 2011; Blomberg and Siegbahn, 2012); see Section 3.4]. The absence of the second binding site E_2 is represented by $\alpha_2 = 1$, as it represents no isotopic fractionation associated with substrate binding.

The preceding derivations show that clumped-isotope distributions for kinetically controlled isotope-pairing reactions are determined by (1) the bulk isotopic abundances at each atom position and (2) the isotopomer-specific fractionation factors for forward reaction. The former is controlled by properties extrinsic to the bond-making chemistry, while the latter is controlled by intrinsic isotope-pairing chemistry. While the sensitivity of clumped-isotope distributions to atomic source might be viewed as a confounding complication, note that many isotope-pairing reactions draw atoms from a common reservoir. For example, in photosynthetic O_2 formation from water, the source reservoir for both oxygen atoms is identical, well-mixed, and effectively infinite. In that case, the clumped-isotope signature primarily reflects the biochemistry of photosynthesis and not the isotopic composition of the source water (Yeung et al., 2015). For N_2 formation from nitric oxide in denitrification, however, the source reservoir is finite and potentially sensitive to environmental conditions [(Yang et al., 2014); see Section 3.4]. Nevertheless, Δ_n values are sensitive to biochemistry at the molecular level. They provide additional information to bulk isotope measurements, potentially offering new ways to quantify the imprints of biogeochemical processes on environmentally meaningful spatial scales.

2.3. Heteronuclear atom association

2.3.1. Irreversible atom association

Are combinatorial effects important when atoms from different isotope systems are bound irreversibly? The irreversible assembly of a heteronuclear diatomic molecule, A–B, expresses combinatorial effects differently from the preceding examples utilizing isotope pairs. To derive a generalized expression, I use a reaction scheme involving A and B atoms, drawn from an infinite reservoir, which bind to substrate-specific sites E_1 and E_2:

$$A + E_1 \rightleftharpoons AE_1 \quad (R6)$$

$$B + E_2 \rightleftharpoons BE_2 \quad (R7)$$

$$AE_1 + BE_2 \rightarrow A\text{–}B + E_1 + E_2 \quad (R8)$$

with similar reactions for each possible isotopic substitution. The isotopic composition of the products is

$${}^{A'\text{–}B}R_{sample} = \frac{[(A'B)]}{[(AB)]} = \frac{[A']}{[A]}\alpha_A \quad (37)$$

$${}^{A\text{–}B'}R_{sample} = \frac{[(AB')]}{[(AB)]} = \frac{[B']}{[B]}\alpha_B \quad (38)$$

$${}^{A'\text{–}B'}R_{sample} = \frac{[(A'B')]}{[(AB)]} = \left(\frac{[A']}{[A]}\alpha_A\right)\left(\frac{[B']}{[B]}\alpha_B\right) \quad (39)$$

For two-isotope systems such as carbon and hydrogen, the stochastic distribution of isotopes in the product is:

$$\begin{aligned} {}^{A'\text{–}B'}R_{stochastic} &= \frac{[A']_p[B']_p}{[A]_p[B]_p} \\ &= \left\{\frac{[(A'B)]+[(A'B')]}{[(AB)]+[(AB')]}\right\}\left\{\frac{[(AB')]+[(A'B')]}{[(AB)]+[(A'B)]}\right\} \\ &= \left(\frac{{}^{A'\text{–}B}R_{sample} + {}^{A'\text{–}B'}R_{sample}}{1+{}^{A\text{–}B'}R_{sample}}\right)\left(\frac{{}^{A\text{–}B'}R_{sample} + {}^{A'\text{–}B'}R_{sample}}{1+{}^{A'\text{–}B}R_{sample}}\right) \\ &= \left({}^{A'\text{–}B}R_{sample}\right)\left({}^{A\text{–}B'}R_{sample}\right) \end{aligned} \quad (40)$$

The expression for $\Delta_{A'\text{–}B'}$ then yields

$$\Delta_{A'\text{–}B'} = \left[\frac{\left({}^{A'\text{–}B}R_{sample}\right)\left({}^{A\text{–}B'}R_{sample}\right)}{\left({}^{A'\text{–}B}R_{sample}\right)\left({}^{A\text{–}B'}R_{sample}\right)} - 1\right] = 0 \quad (41)$$

With only one atom and two isotopes of each type in the molecule, the above expression is trivial in hindsight: $\Delta_{A'\text{–}B'}$ values from irreversible heteronuclear association are always zero, i.e., there is no combinatorial effect.

The expression also holds for multi-isotope systems. For example, when A^* and B^* isotopes are also relevant, then the calculated stochastic distribution does not change:

$$\begin{aligned} {}^{A'\text{–}B'}R_{stochastic} &= \left(\frac{{}^{A'\text{–}B}R_{sample} + {}^{A'\text{–}B'}R_{sample} + {}^{A'\text{–}B^*}R_{sample}}{1+{}^{A\text{–}B'}R_{sample} + {}^{A\text{–}B^*}R_{sample}}\right) \\ &\quad \times \left(\frac{{}^{A\text{–}B'}R_{sample} + {}^{A'\text{–}B'}R_{sample} + {}^{A^*\text{–}B'}R_{sample}}{1+{}^{A'\text{–}B}R_{sample} + {}^{A^*\text{–}B}R_{sample}}\right) \\ &= \left({}^{A'\text{–}B}R_{sample}\right)\left({}^{A\text{–}B'}R_{sample}\right) \end{aligned} \quad (42)$$

Indeed, one can show that $\Delta_n = 0$ for all possible multiply-substituted isotopologues in this heteronuclear diatomic system. These systematics are a manifestation of the lack of symmetry across the A–B bond: the "lop-sidedness" that can arise during asymmetric A′–A isotopomer formation cannot develop during A–B formation. The B atom does not affect the stochastic distribution of the A atom, nor vice versa. In the language of the example used at the beginning of Section 2, the left hand might choose between red and green apples, but the right hand chooses between red and green tomatoes; there is always only one of each fruit in a pair, no matter the color.

Thus, the first-order combinatorial effect for irreversible bond formation between two different species is to yield $\Delta_{A'\text{–}B'} = 0$. Chemical effects are important, but they depend on the system (see below).

2.3.2. Atom association controlled by the A–B transition state

Finally, I examine the association of a heteronuclear diatomic molecule through a transition state, i.e.,

$$AE_1 + BE_2 \rightleftharpoons (E_1A\text{–}BE_2)^{\ddagger} \rightarrow A\text{–}B + E_1 + E_2 \quad (R9)$$

where the isotopologue abundances are analogous to those in Eqs. (31) and (32):

$$^{A'-B}R_{sample} = \frac{[(A'B)]}{[(AA)]} = {}^{A}\alpha_{k'}\left(\frac{[A']}{[A]}\right)\alpha_A \quad (43)$$

$$^{A-B'}R_{sample} = \frac{[(AB')]}{[(AA)]} = {}^{B}\alpha_{k'}\left(\frac{[B']}{[B]}\right)\alpha_B \quad (44)$$

$$^{A'-B'}R_{sample} = \frac{[(A'B')]}{[(AA)]} = \alpha_{k''}\left(\frac{[A'][B']}{[A][B]}\right)\alpha_A\alpha_B \quad (45)$$

In Eqs. 43–45, the subscripts and superscripts A and B denote the atom to which the isotopic fractionation factor α applies. For example, ${}^{A}\alpha_{k'}$ is the isotopomer fractionation factor for producing A′–B in reaction R9, whereas ${}^{B}\alpha_{k'}$ applies to A–B′. The stochastic distribution is therefore:

$$\begin{aligned} ^{A'-B'}R_{stochastic} &= \left(\frac{^{A'-B}R_{sample} + {}^{A'-B'}R_{sample}}{1 + {}^{A-B'}R_{sample}}\right)\left(\frac{^{A-B'}R_{sample} + {}^{A'-B'}R_{sample}}{1 + {}^{A'-B}R_{sample}}\right) \\ &= \left[\frac{\left({}^{A}\alpha_{k'}\frac{[A']}{[A]}\alpha_A\right)\left(1 + \frac{\alpha_{k''}}{{}^{A}\alpha_{k'}}\frac{[B']}{[B]}\alpha_B\right)}{1 + {}^{B}\alpha_{k'}\frac{[B']}{[B]}\alpha_B}\right] \\ &\quad \times \left[\frac{\left({}^{B}\alpha_{k'}\frac{[B']}{[B]}\alpha_B\right)\left(1 + \frac{\alpha_{k''}}{{}^{B}\alpha_{k'}}\frac{[A']}{[A]}\alpha_A\right)}{1 + {}^{A}\alpha_{k'}\frac{[A']}{[A]}\alpha_A}\right] \end{aligned} \quad (46)$$

And the clumped isotope distribution is

$$\Delta_{A'-B'} = \left[\left(\frac{\alpha_{k''}}{{}^{A}\alpha_{k'}{}^{B}\alpha_{k'}}\right)\frac{\left(1 + {}^{B}\alpha_{k'}\frac{[B']}{[B]}\alpha_B\right)\left(1 + {}^{A}\alpha_{k'}\frac{[A']}{[A]}\alpha_A\right)}{\left(1 + \frac{\alpha_{k''}}{{}^{A}\alpha_{k'}}\frac{[B']}{[B]}\alpha_B\right)\left(1 + \frac{\alpha_{k''}}{{}^{B}\alpha_{k'}}\frac{[A']}{[A]}\alpha_A\right)} - 1\right] \quad (47)$$

$$= \left[\left(\frac{\alpha_{k''}}{{}^{A}\alpha_{k'}{}^{B}\alpha_{k'}}\right)\frac{\left(1 + {}^{B}\alpha_{k'}{}^{B'}R\right)\left(1 + {}^{A}\alpha_{k'}{}^{A'}R\right)}{\left(1 + \frac{\alpha_{k''}}{{}^{A}\alpha_{k'}}{}^{B'}R\right)\left(1 + \frac{\alpha_{k''}}{{}^{B}\alpha_{k'}}{}^{A'}R\right)} - 1\right] \quad (48)$$

with ${}^{A'}R = \alpha_A[A']/[A]$ and ${}^{B'}R = \alpha_B[B']/[B]$ for the reactants. Systems of three isotopes or more have similar, but analogous expressions not shown here. Similar to the isotope-pairing systematics described in Section 2.2.3, $\Delta_{A'-B'}$ values depend on the bulk abundance of both A and B in a nonlinear way. They are shown for several moieties of carbon species in Fig. 4 (left panel). As the bulk abundance of the rare isotopes increases (i.e., increasing magnitude of ${}^{A'}R$ and/or ${}^{B'}R$ values), $\Delta_{A'-B'}$ values become less sensitive to properties of the transition state.

This tempering of intrinsic kinetic fractionation factors is one of two combinatorial effects for isotope clumping between two different species. The second effect is a dependence of $\Delta_{A'-B'}$ values on the fractionation factors relevant to the singly-substituted products (${}^{A}\alpha_{k'}$ and ${}^{B}\alpha_{k'}$ values). For a given isotope-clumping tendency expressed by the transition state, i.e., constant $\alpha_{k''}/({}^{A}\alpha_{k'}{}^{B}\alpha_{k'})$ ratios, different ${}^{A}\alpha_{k'}$ and ${}^{B}\alpha_{k'}$ values result in offsets in $\Delta_{A'-B'}$ values. These offsets depend on the bulk abundance of each atom: they increase in magnitude from ~0.01‰ for the relatively rare ^{13}C–^{18}O moiety to ~0.1‰ for the more abundant ^{13}C–^{37}Cl moiety when the bulk-isotope fraction factors are between 0.995 and 1.005 (see Fig. 4, right panel).

In the low-abundance limit, Eq. (48) becomes simply related to the properties of the transition state:

$$\Delta_{A'-B'} \approx \left[\frac{\alpha_{k''}}{{}^{A}\alpha_{k'}{}^{B}\alpha_{k'}} - 1\right] \quad (49)$$

One must exercise caution in applying this approximation when making *ab initio* predictions for heteronuclear isotope combinations, however: While Eqs. (47) and (48) show that $\Delta_{A'-B'}$ is largely determined by the chemistry of the reactive transition state, $\Delta_{A'-B'}$ values are much more sensitive to rare-isotope abundance than $\Delta_{A'-A'}$ values are (Section 2.2.3).

3. BIOGEOCHEMICAL APPLICATIONS

The generalized derivations in the preceding section reveal a fundamental feature of clumped-isotope

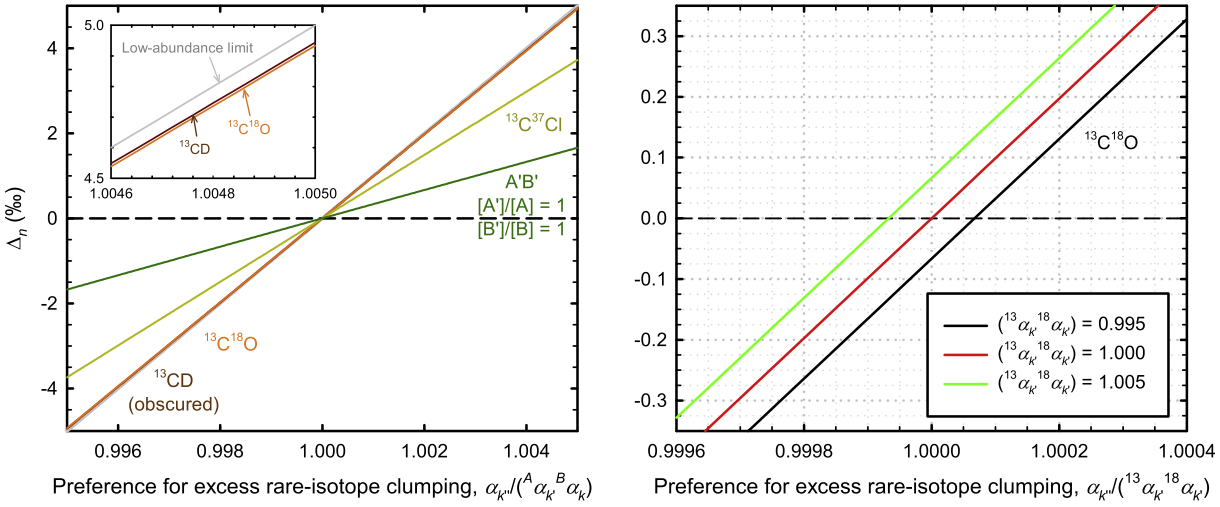

Fig. 4. Influence of rare-isotope abundance on product Δ_n values of heteronuclear moieties. Similar to the isotope-pairing case, rare-isotope clumping in heteronuclear moieties is strongly dependent on intrinsic kinetic clumping/anticlumping preferences, i.e., $\alpha_{ki}/({}^{A}\alpha_{k'}{}^{B}\alpha_{k'})$ in Eqs. (47) and (48). (Left) Increasing abundance of the doubly-substituted moiety reduces the sensitivity of Δ_n values to kinetic clumping/anticlumping preferences. (Right) Isotopic preferences relevant to the singly-substituted species will offset Δ_n vs. $\alpha_{k''}/({}^{A}\alpha_{k'}{}^{B}\alpha_{k'})$ curves, as shown for $^{13}C^{18}O$ moieties. Note the difference in scale on the right-hand plot.

geochemistry: kinetic signatures depend both combinatorial and chemical-kinetic factors. For isotope pairing, a "clumped" isotope distribution (i.e., $\Delta_n > 0$) is produced when the chemistry of the transition state favors the formation of rare-atom pairs enough to overcome the combinatorial tendencies favoring the opposite outcome. Unequal abundances of rare isotopes at different molecular positions tend to reduce Δ_n values from the transition-state's preference for rare-isotope clumping. The abundance of the rare isotope has an influence as well.

In heteronuclear systems with a unique atom B (e.g., CO, NO_3^-, SO_4^{2-}), the lack of symmetry-based peculiarities on A′–B′ clumping reduces the variability of combinatorial factors. Yet, isotope pairs within those molecules (e.g., O–O pairs in NO_3^-, SO_4^{2-}) will still be subject to the combinatorial factors described above. The expressions for Δ_n values derived in Section 2 are summarized in Table 1.

How will Δ_n values vary in nature? Isotope pairs in diatomic molecules produced biochemically, such as O_2 from photosynthesis, H_2 from nitrogen fixation (Hadfield and Bulen, 1969; Scranton et al., 1987), and N_2 from denitrification are sensitive to combinatorial effects in their clumped isotope distributions, but the expression of combinatorial effects in these systems will depend on the magnitude of intrinsic kinetic isotope effects. In polyatomic molecules, combinatorial effects are not as obvious: While analytical expressions exist for the sequential molecular assembly of polyatomic molecules, they are quite complex (even for A–B–A molecules) because of the number of possible isotopomer products. However, combinatorial effects apply during each atomic addition step, so the insights gained from examining diatomic systems apply generally to the synthesis of polyatomic molecules. Furthermore, the occurrence of isotope pairs within any polyatomic molecule can be described by the systematics outlined in Section 2, regardless of their bonding partners (e.g., two hydrogen atoms bound to two different carbon atoms).

For the general case in which the clumped-isotope distribution in polyatomic molecules is inherited partially from other processes or reservoirs, the Δ_n value of the molecule depends on (1) the inherited isotopic composition of the reactants, (2) combinatorial factors, and (3) properties of the bond-forming transition state. Consider the irreversible and non-fractionating addition (after Section 2.3.1) of an O-atom to a CO fragment of arbitrary $\Delta_{13C-18O} = +1‰$ to form CO_2:

$$O + CO(\Delta_{13C-18O} = 1‰) \rightarrow CO_2(\Delta_{13C-18O} \approx 0.5‰) \quad (R10)$$

Under these assumptions, the $\Delta_{13C-18O}$ value for CO_2 would be approximately half that of the CO fragment, i.e., ~0.5‰, because the inherited CO fragment with "clumped" composition constitutes half the total number of C—O bonds; the other C—O bonds are added according to chance alone (Eq. (41)), with secondary isotope effects here assumed to be negligible. The $\Delta_{18O-18O}$ value, in contrast, is determined combinatorially, as the reaction chemistry imposed here resembles the irreversible isotope-pairing case outlined in Section 2.2. Relative-rate predictions for reaction (R10) indicate that its chemical isotope effects are quite large (Gao and Marcus, 2007), so the combinatorial effects discussed in this simplified example should be considered endmember effects.

I reiterate here that this paper is not meant to be an exhaustive account of all possible clumped-isotope distributions arising from kinetically controlled reactions. It is meant instead to provide a framework in which one can examine the effects of these reactions on the clumped-isotope composition of geochemically interesting molecules. These concepts are, in some sense, already incorporated into more sophisticated formulations of biosynthesis (Hayes, 2001; Valentine et al., 2004; Brunner and Bernasconi, 2005; Stolper et al., 2015; Wang et al., 2015), but the concepts described here offer a more general understanding of how to interpret and envision clumped-isotope distributions in nature.

3.1. Marine oxygen cycling

The oxidation of two water molecules by plants and algae to form molecular oxygen occurs at the oxygen-evolving complex of the photosystem II enzyme. It catalyzes the following four-electron oxidation:

Table 1
Summary of expressions for isotope pairing and heteronuclear isotope clumping for two-isotope systems.

Reaction	$\Delta_n + 1$ (single, infinite atom reservoir)	$\Delta_n + 1$ (arbitrary atom reservoirs)	Section
Irreversible bond formation			
$A'E_1 + A'E_2 \rightarrow A'–A' + E_1 + E_2$ (two-isotope system)	$\frac{\alpha_1\alpha_2\left[2+\frac{[A']}{[A]}(\alpha_1+\alpha_2)\right]^2}{\left[\alpha_1+\alpha_2+2\frac{[A']}{[A]}\alpha_2\alpha_1\right]^2}$	$\frac{{}'R_1{}'R_2(2+{}'R_1+{}'R_2)^2}{({}'R_1+{}'R_2+2{}'R_1{}'R_2)^2}$	2.2.1
$A'E_1 + A'E_2 \rightarrow A'–A' + E_1 + E_2$ (three-isotope system)	$\frac{\alpha_1\alpha_2\left[2+\frac{[A^*]}{[A]}(\alpha_{1^*}+\alpha_{2^*})+\frac{[A']}{[A]}(\alpha_1+\alpha_2)\right]^2}{\left[\alpha_1+\alpha_2+2\frac{[A']}{[A]}\alpha_2\alpha_1+\frac{[A^*]}{[A]}(\alpha_{1^*}\alpha_2+\alpha_1\alpha_{2^*})\right]^2}$	$\frac{{}'R_1{}'R_2(2+{}^*R_1+{}^*R_2+{}'R_1+{}'R_2)^2}{({}'R_1+{}'R_2+2{}'R_1{}'R_2+{}^*R_1{}'R_2+{}'R_1{}^*R_2)^2}$	2.2.2
$A'E_1 + B'E_2 \rightarrow A'–B' + E_1 + E_2$	1	1	2.3.1
Bond formation controlled by transition state			
$A'E_1 + A'E_2 \rightleftharpoons (E_1A'–A'E_2)^{\ddagger} \rightarrow A'–A' + E_1 + E_2$	$\frac{\alpha_1\alpha_2\alpha_{k''}\left\{2+\frac{[A']}{[A]}(\alpha_1\alpha_{k1'}+\alpha_2\alpha_{k2'})\right\}^2}{\left\{\alpha_1\alpha_{k1'}+\alpha_2\alpha_{k2'}+2\frac{[A']}{[A]}\alpha_1\alpha_2\alpha_{k''}\right\}^2}$	$\frac{{}'R_1{}'R_2\alpha_{k''}(2+{}'R_1\alpha_{k1'}+{}'R_2\alpha_{k2'})^2}{({}'R_1\alpha_{k1'}+{}'R_2\alpha_{k2'}+2{}'R_1{}'R_2\alpha_{k''})^2}$	2.2.3
$A'E_1 + B'E_2 \rightleftharpoons (E_1A–BE_2)^{\ddagger} \rightarrow A'–B' + E_1 + E_2$	$\left(\frac{\alpha_{k''}}{{}^{A}\alpha_{k'}{}^{B}\alpha_{k'}}\right)\frac{\left(1+{}^{B}\alpha_{k'}\frac{[B']}{[B]}\alpha_B\right)\left(1+{}^{A}\alpha_{k'}\frac{[A']}{[A]}\alpha_A\right)}{\left(1+\frac{\alpha_{k''}}{{}^{A}\alpha_{k'}}\frac{[B']}{[B]}\alpha_B\right)\left(1+\frac{\alpha_{k''}}{{}^{B}\alpha_{k'}}\frac{[A']}{[A]}\alpha_A\right)}$	$\left(\frac{\alpha_{k''}}{{}^{A}\alpha_{k'}{}^{B}\alpha_{k'}}\right)\frac{\left(1+{}^{B}\alpha_{k'}{}^{B'}R\right)\left(1+{}^{A}\alpha_{k'}{}^{A'}R\right)}{\left(1+\frac{\alpha_{k''}}{{}^{A}\alpha_{k'}}{}^{B'}R\right)\left(1+\frac{\alpha_{k''}}{{}^{B}\alpha_{k'}}{}^{A'}R\right)}$	2.3.2

$$2H_2O + 4h\nu \rightarrow O_2 + 4H^+ + 4e^- \quad \text{(R11)}$$

The reaction is a multi-step redox mechanism (McEvoy and Brudvig, 2006) that does not fractionate ^{17}O or ^{18}O during production of O_2 from the water substrate (Guy et al., 1993; Helman et al., 2005). This absence of bulk isotopic fractionation suggests that $\alpha_{k1'} \approx 1$ and $\alpha_{k2'} \approx 1$ in Eq. (33), i.e., photosynthetic O—O bond formation has a loose transition state. If O—O bond formation is a mass-dependent process, then $\alpha_{k''} \sim \alpha_{k1'}\alpha_{k2'}$, resulting in $\alpha_{k''}/(\alpha_{k1'}\alpha_{k2'})$ values that are close to unity as well (Young et al., 2002), and no preference for rare-isotope pairing beyond chance statistics; O—O isotope pairing may therefore be described well by Eqs. (20) and (23).

Isotope-labeling experiments have shown that water binds to two non-equivalent binding sites on the enzyme (Hillier and Wydrzynski, 2008; Rapatskiy et al., 2012). Eqs. (20) and (23) therefore predict that $\Delta_{35} < 0$ and $\Delta_{36} < 0$ for the evolved O_2. Yeung et al. (2015) presented data from a closed terrarium experiment utilizing water hyacinths (*Eichhorniae crassipes* on 12 h/12 h light/dark cycles) that showed Δ_{35} and Δ_{36} values evolving toward a steady-state at the stochastic distribution of isotopes ($\Delta_{35} = 0$ and $\Delta_{36} = 0$). They observed that dark incubations increased Δ_{35} and Δ_{36} values and consequently inferred that photosynthesis must generate O_2 with $\Delta_{35} < 0$ and $\Delta_{36} < 0$ to compensate. Whether this clumped-isotope deficit is purely combinatorial in origin or also influenced by subtle kinetic isotope effects remains to be tested; combinatorial effects are unlikely to yield O_2 with $\Delta_{35} < -0.5‰$ and $\Delta_{36} < -1‰$, however, because of the typical magnitude of oxygen-isotope effects associated with enzyme-substrate binding [i.e., $\alpha = 0.97 - 1.03$; (Angeles-Boza and Roth, 2012; Angeles-Boza et al., 2014)].

While the clumped-isotope signatures of photosynthesis have not yet been determined unequivocally (values as low as $\Delta_{35} = -5‰$ and $\Delta_{36} = -10‰$ cannot yet be ruled out), the clumped-isotope composition of O_2 can nonetheless be further developed as a tracer of marine oxygen cycling. A clumped-isotope approach would complement oxygen-isotope methods for determining primary productivity (Bender and Grande, 1987; Quay et al., 1993; Luz and Barkan, 2000; Juranek and Quay, 2013) because Δ_{35} and Δ_{36}, unlike other oxygen-isotope tracers, would be insensitive to the isotopic composition of the photosynthetic source water. They would allow one to solve for the end-member isotopic composition of photosynthetic O_2 in different environments, which can be uncertain (Eisenstadt et al., 2010; Kaiser, 2011; Luz and Barkan, 2011). Furthermore, it may provide more constraints on the fate of photosynthetically produced oxygen (Kaiser, 2011; Nicholson et al., 2014). Using an endmember composition of $\Delta_{36,p} = {}^{-}0.4 - {}^{-}10‰$ for photosynthetic O_2, a 10% mixture of photosynthetic O_2 with atmospheric O_2 in the upper ocean [$\Delta_{36,air} = 2‰$ (Yeung et al., 2014)] would yield signals between 0.2‰ and 1‰ in magnitude, within detection limits of current methods (Yeung et al., 2014). Respiration and gas exchange can cause additional isotopologue fractionation, however. Future development of this approach may yield insights into the oxygen budget of the deep ocean (Bender, 1990; Levine et al., 2009).

3.2. Methanogenesis

Methanogenesis from CO_2 and acetate progresses through reversible two-electron reductions coupled with hydrogen-atom addition (Rouvière and Wolfe, 1988). These hydrogen atoms are correlated only through secondary isotope effects, resulting in a strong combinatorial effect when the reversibility is low and methane production is strongly favored. If H_2O ultimately provides all of the hydrogen atoms on methane (Whiticar et al., 1986; Valentine et al., 2004), one might expect the combinatorial effects on $\Delta^{12}CH_2D_2$ values to be dominated by the intrinsic deuterium kinetic fractionation factors, rendering $\Delta^{12}CH_2D_2$ values insensitive to the isotopic composition of the source water. In contrast, if one or more of the hydrogen atoms on methane comes from a different source, as may be the case for acetoclastic methanogenesis (CH_4 production from acetate substrates), then both enzymatic and inherited fractionation factors will influence $\Delta^{12}CH_2D_2$ values of the methane evolved. Reversibility in methane production may also drive $\Delta^{12}CH_2D_2$ values toward equilibrium values, which are greater than zero (Cao and Liu, 2012; Stolper et al., 2014a, b, 2015; Webb and Miller, 2014; Wang et al., 2015).

The $^{13}CH_3D$ clumped-isotope composition of methane ($\Delta^{13}CH_3D$) has been applied to distinguish thermogenic and biogenic sources of methane (Stolper et al., 2014a, 2015; Wang et al., 2015). It can express both equilibrium and non-equilibrium signatures, depending on hydrogen availability; H_2-replete conditions seem to promote kinetically constrained reactions, resulting in methane formed with $\Delta^{13}CH_3D$ values as low as $-5‰$ (Stolper et al., 2015; Wang et al., 2015). The equations derived in Section 2.3 suggest that the source of these large anticlumped $^{13}CH_3D$ signatures is unlikely to be combinatorial; in clumps of two dissimilar atomic species, anticlumped isotope distributions arise only from kinetic isotope effects.

The $\Delta^{13}CH_3D$ and $\Delta^{12}CH_2D_2$ values in methane can therefore complement each other in biogeochemical studies. Clumped-isotope disequilibria due to kinetic effects will be correlated on a plot of $\Delta^{13}CH_3D$ vs. $\Delta^{12}CH_2D_2$ (Young et al., 2011), while D–D combinatorial effects will only affect $\Delta^{12}CH_2D_2$ and other multiply-deuterated methanes. Using $^{D}\alpha$ values between 0.9 and 1.1, Eq. (13) suggests that the magnitude of combinatorial effects can be as large as $-10‰$ in $\Delta^{12}CH_2D_2$, comparable in magnitude to $\Delta^{12}CH_2D_2$ values expected at isotopic equilibrium (Young et al., 2011). Combinatorial effects may therefore be important to the relative abundances of multiply-deuterated methanes under kinetically controlled conditions. Application of such a multiple-isotopologue technique may help disentangle the ubiquitous chemical and reservoir effects relevant to biogeochemical methane cycling.

3.3. Biological nitrogen fixation

Molecular hydrogen is a byproduct of biological nitrogen fixation (Hadfield and Bulen, 1969; Scranton et al.,

1987). In the molybdenum-containing variant of nitrogenase, hydrogen is believed to be evolved from hydrides (H^-) bound to the catalytic iron-molybdenum cofactor (FeMo-co) after N_2 binds to one of the Fe metal centers of the cluster (Hoffman et al., 2014). While the reaction is part of a multi-step sequence, its essential elements with respect to isotope pairing are:

$$\mathbf{H^-}\text{–[FeMo-co]–}\mathbf{H^-} + N_2 \rightleftharpoons \mathbf{H_2} + \text{[FeMo-co]–}N_2 \qquad \text{(R12)}$$

Hydrogen evolution is reversible (Yang et al., 2013; Lukoyanov et al., 2015), but both combinatorial and chemical-kinetic factors could be important for the clumped-isotope distribution of H_2. In particular, variability in H_2 partial pressure may modulate the reversibility of reaction R12 and its attendant isotopic fractionation, such as in soils where partial pressures of H_2 can be higher than those in the free atmosphere (Conrad and Seiler, 1979). Consequently, clumped-isotope compositions of H_2 evolved from high- and low-H_2 environments may differ. In addition, hydrogenase and nitrogenase enzymes can catalyze isotope exchange between H_2 and H_2O (Jackson et al., 1968; Whiticar et al., 1986; Valentine et al., 2004; Vignais, 2005). If these isotope-exchange reactions are important, then combinatorial signatures will be negligible compared to those caused by equilibrium and kinetic processes [e.g., $\Delta_4 \sim 200‰$ at 25 °C equilibrium; (Richet et al., 1977; Yang et al., 2012)]. If isotope exchange is rapid and complete, then H_2 from nitrogen fixation may express a clumped-isotope composition more consistent with H_2 formation temperatures and the environments where nitrogen is fixed.

Nevertheless, the marine nitrogen budget remains uncertain (Mahaffey et al., 2005; Deutsch et al., 2007; Galloway et al., 2008; Eugster and Gruber, 2012) in part because past measurements of marine nitrogen fixation may have be inaccurate (Grosskopf et al., 2012); additional *in situ* estimates would be useful. Observations of H_2 supersaturation in the mixed layer (Moore et al., 2009, 2014; Wilson et al., 2013) suggest that the isotopic composition of H_2 may record information about nitrogen fixation.

3.4. Conversion of fixed nitrogen to N_2 and N_2O

Nitrogen-nitrogen bonds are formed during denitrification, nitrification, and anaerobic ammonia oxidation (anammox). During biological denitrification, nitrate (NO_3^-) is reduced to dinitrogen (N_2) through a series of intermediate steps involving nitrite (NO_2^-), nitric oxide (NO), and nitrous oxide (N_2O), i.e.,

$$NO_3^- \rightarrow NO_2^- \rightarrow NO \rightarrow N_2O \rightarrow N_2 \qquad \text{(R13)}$$

The reduction $2\,NO + 2H^+ + 2e^- \rightarrow N_2O + H_2O$ is the relevant reaction that pairs nitrogen atoms; it sets the relative abundance of $^{15}N{-}^{15}N$ bonds (i.e., the Δ_{30} value) in N_2O, which is then inherited by N_2 (Ostrom et al., 2007). The reaction is catalyzed by the enzyme nitric oxide reductase (NOR), which has different variants in bacteria and fungi. Each variant utilizes a different mechanism (Fig. 5), which could impart its signature on the Δ_{30} values of N_2O and/or N_2 produced (Shiro et al., 1995, 2012; Riplinger and Neese, 2011; Blomberg and Siegbahn, 2012).

These Δ_{30} values and the intramolecular distribution of ^{15}N in N_2O (Toyoda et al., 2005) share a common origin, i.e., enzymatic and chemical fractionation factors for N—N bond formation, so the theory and observations regarding the site preference of ^{15}N in N_2O are also germane to Δ_{30} values in N_2O and N_2. I will examine them below.

A variety of denitrifiers evolve N_2O with asymmetric ^{15}N site preferences ($SP = \delta^{15}N_{central} - \delta^{15}N_{terminal}$). For bacterial denitrification, measurements of pure cultures range from $SP = -10‰$ to $\sim 0‰$ (Toyoda et al., 2005; Frame and Casciotti, 2010; Mothet et al., 2013; Yamazaki et al., 2014). Experiments on fungal denitrification show a larger and more consistent site preference [e.g., $SP = 37‰$; (Sutka et al., 2008)], although its magnitude is species- and culture-dependent (Rohe et al., 2014). Nitrification by ammonia- and methane-oxidizing bacteria and archaea can also produce N_2O through hydroxylamine (NH_2OH) and NO intermediates. The $NH_2OH + NO$ pathway ["nitrifier-denitrification" (Ritchie and Nicholas,

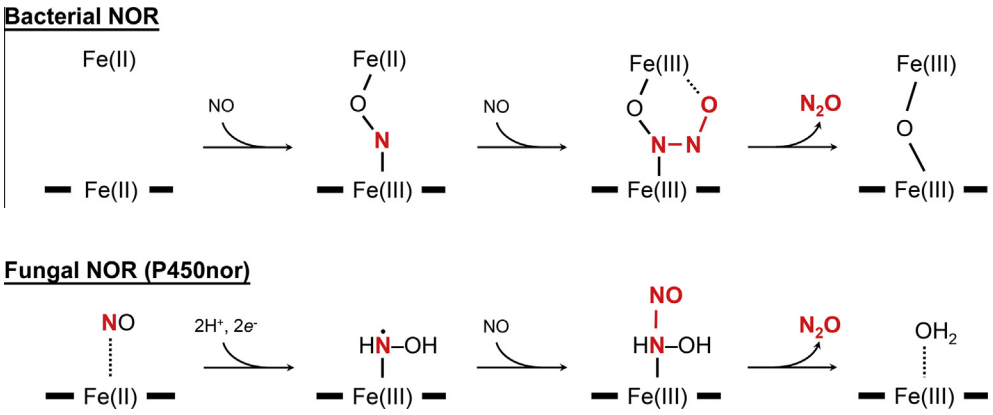

Fig. 5. Candidate mechanisms for N_2O production by bacterial and fungal NOR, which likely lead to characteristic $^{15}N{-}^{15}N$ clumping in the products. The bacterial NOR mechanism was proposed by Blomberg and Siegbahn (2012) while the fungal (P450nor) mechanism was proposed by Riplinger and Neese (2011). The iron atoms represent two sites on the enzyme that are involved in N—N bond formation. Atoms that comprise the product N_2O are highlighted in red. (For interpretation of the references to colour in this figure legend, the reader is referred to the web version of this article.)

1972)] results in a ^{15}N site preference similar to that of fungal denitrification (Sutka et al., 2003; Santoro et al., 2011; Jung et al., 2014; Yamazaki et al., 2014), while the NO + NO pathway results in a ^{15}N site preference similar to that for bacterial denitrification (Sutka et al., 2008; Frame and Casciotti, 2010).

These site preferences are mechanism-specific, but they can be evaluated within the framework of reaction R5 in Section 2.2.3. In general, Δ_{30} values in the N_2O and N_2 products are a convolution of site-specific $^{15}N/^{14}N$ contrast and kinetic isotope effects for N—N bond formation. Using ^{15}N fractionation factors of order 0.99–1.04 [e.g., (Frame and Casciotti, 2010; Yamazaki et al., 2014; Yang et al., 2014)], combinatorial clumped-isotope effects are predicted to deplete ^{15}N—^{15}N isotopomers of N_2O and N_2 by up to −0.6‰ relative to the kinetic isotope effects associated with ^{15}N—^{15}N pairing. Future measurements of Δ_{30} values will reveal whether the ^{15}N site preference in N_2O is caused by binding interactions between NO and NOR, kinetic isotope effects in N—N bond formation, or both.

Anaerobic ammonium oxidation is a third important pathway through which N—N bonds are formed in nature. Unlike the previous mechanisms, the anammox pathway combines NO and ammonium (NH_4^+) to form hydrazine (N_2H_4) before being oxidized to N_2 (Kartal et al., 2011):

$$NO_2^- \rightarrow NO + NH_4^+ \rightarrow N_2H_4 \rightarrow N_2 \quad \text{(R14)}$$

Little is known about the enzymatic steps leading to N_2H_4 formation, but the two different nitrogen pools for NO_2^- and NH_4^+ have different $\delta^{15}N$ compositions. In oxygen-deficient areas where anammox is particularly active, NO_2^- and NH_4^+ could differ in composition by many tens of per mil, because enzyme-catalyzed nitrogen-isotope exchange may deplete $\delta^{15}N$ in NO_2^- by as much as −60‰ relative to NO_3^- (Brunner et al., 2013). Furthermore, experimental cultures of anammox bacteria were observed to have isotopic fractionation factors for NO_2^- and NH_4^+ assimilation that differed by ~10‰ (Brunner et al., 2013). Therefore, combinatorial depletions in Δ_{30} are expected for anammox-derived N_2: Using a 10–60‰ difference in $\delta^{15}N$ between the NO_2^- and NH_4^+ in R14, Eq. (33) predicts that combinatorial effects will reduce the Δ_{30} value of N_2 by $^-$0.02–$^-$0.9‰ relative to chemical-kinetic preferences. The precise Δ_{30} value relative to that produced by other N_2 sources is difficult to estimate, however, because of a paucity of open-ocean $\delta^{15}N$–NH_4^+ measurements (Altabet, 2006), nutrient cycling mechanisms in unique microenvironments (Prokopenko et al., 2013), and poorly known enzyme-^{15}N fractionation factors.

In all of these mechanisms for nitrogen loss, molecular details about both the N—N bond-forming step and the substrate-determining steps will likely influence Δ_{30} values in N_2O and N_2 products. Clumped-isotope measurements of natural N_2O and N_2 may clarify the role of bacterial and fungal nitrogen-loss mechanisms in soils (Seitzinger et al., 2006; Galloway et al., 2008), as well as the role of anammox in the global nitrogen cycle (Galloway et al., 2004; Kuypers et al., 2005; Gruber and Galloway, 2008). Quantification of these nitrogen-loss mechanisms has been challenging (Risgaard-Petersen et al., 2003; Davidson and Seitzinger, 2006), and clumped-isotope measurements may yield new insights. The magnitude of expected equilibrium and combinatorial clumped-isotope signatures is similar [of order ±1‰; (Wang et al., 2004)], and kinetic isotope effects may be larger in magnitude, so new constraints on nitrogen cycling may emerge if Δ_{30} values can be measured with analytical precision of ±0.1‰.

4. CONCLUSIONS

Clumped-isotope distributions are sensitive to physical (e.g., diffusive), chemical (e.g., transition-state), and combinatorial isotope effects. Chemical and combinatorial effects, in particular, are intertwined during bond formation: Combinatorial effects tend to decrease Δ_n values of the products in isotope pairing reactions. These effects arise from unequal isotopic preferences during substrate selection. A secondary combinatorial effect is related to rare-isotope abundance: The sequestration of rare isotopes into multiply-substituted moieties reduces the sensitivity of the clumped-isotope distribution to both chemical and combinatorial factors. Explicit accounting of these combinatorial effects is required for high-precision comparison of predicted clumped-isotope signatures (e.g., from *ab initio* calculations) and those observed in nature.

Furthermore, I find that recent observations of non-equilibrium clumped-isotope signatures in CH_4 and O_2 (Stolper et al., 2014a, 2015; Wang et al., 2015; Yeung et al., 2015) originate from two different phenomena. Anticlumped distributions of $^{13}CH_3D$ in CH_4 are minimally affected by purely combinatorial clumped-isotope effects; chemical-kinetic isotope effects control the number of ^{13}C–D isotope clumps relative to the stochastic distribution. In contrast, photosynthetic O_2 is most likely affected by combinatorial clumped-isotope effects, resulting in anticlumped $^{18}O^{18}O$ and $^{17}O^{18}O$ distributions. Mechanisms of N—N bond formation relevant to the global nitrogen cycle suggest that clumped-isotope distributions in N_2O and N_2 will carry diverse biochemical signatures. While not discussed in detail here, non-equilibrium distributions of D–D, ^{15}N–^{15}N, and ^{13}C–^{13}C isotope pairs in biogenic organic molecules could conceivably be explored as process-specific isotope signatures in the fossil record, provided the molecules are produced from kinetically controlled biosynthetic pathways and the moieties of interest are resistant to diagenetic alteration.

Finally, combinatorial effects in isotope pairing are not unique to bond-forming chemistry. While bond-rupturing chemistry and bond-preserving (e.g., crystallization) chemistry cannot distinguish symmetrically equivalent molecular isotopomers, they may express preferences for position-specific isotopic substitutions within larger, less symmetric molecules.

ACKNOWLEDGEMENTS

I thank Jeanine Ash, Edwin Schauble, and Ed Young for stimulating discussions that led to this manuscript being conceived, Shuning Li and Eric Hegg for comments on the manuscript, and Ed Young for coming up with the term "combinatorial" to describe the clumped-isotope effects described herein. I also thank Shuhei

Ono and two anonymous reviewers for their detailed comments. This research was supported in part by the National Science Foundation Low-Temperature Geochemistry program (EAR-1349182).

REFERENCES

Affek H. P. (2013) Clumped isotopic equilibrium and the rate of isotope exchange between CO_2 and water. *Am. J. Sci.* **313**, 309–325.

Affek H. P. and Eiler J. M. (2006) Abundance of mass-47 CO_2 in urban air, car exhaust and human breath. *Geochim. Cosmochim. Acta* **70**, 1–12.

Affek H. P. and Zaarur S. (2014) Kinetic isotope effect in CO_2 degassing: Insight from clumped and oxygen isotopes in laboratory precipitation experiments. *Geochim. Cosmochim. Acta* **143**, 319–330.

Affek H. P., Bar-Matthews M., Ayalon A., Matthews A. and Eiler J. M. (2008) Glacial/interglacial temperature variations in Soreq cave speleothems as recorded by 'clumped isotope' thermometry. *Geochim. Cosmochim. Acta* **72**, 5351–5360.

Affek H. P., Matthews A., Ayalon A., Bar-Matthews M., Bursyyn Y., Zaarur S. and Zilberman T. (2014) Accounting for kinetic isotope effects in Soreq Cave (Israel) speleothems. *Geochim. Cosmochim. Acta* **143**, 303–318.

Affek H. P., Xu X. and Eiler J. M. (2007) Seasonal and diurnal variations of $^{13}C^{18}O^{16}O$ in air: initial observations from Pasadena, CA. *Geochim. Cosmochim. Acta* **71**, 5033–5043.

Altabet M. A. (2006) Isotopic tracers of the marine nitrogen cycle: present and past. In *Handbook of Environmental Chemistry* (ed. J. K. Volkman). Springer, Berlin, pp. 251–293.

Angeles-Boza A. M. and Roth J. P. (2012) Oxygen kinetic isotope effects upon catalytic water oxidation by a monomeric ruthenium complex. *Inorg. Chem.* **51**, 4722–4729.

Angeles-Boza A. M., Ertem M. Z., Sarma R., Ibañez C. H., Maji S., Llobet A., Cramer C. J. and Roth J. P. (2014) Competitive oxygen-18 kinetic isotope effects expose O–O bond formation in water oxidation catalysis by monomeric and dimeric ruthenium complexes. *Chem. Sci.* **5**, 1141–1152.

Bender M. L. (1990) The $\delta^{18}O$ of dissolved O_2 in seawater: a unique tracer of circulation and respiration in the deep sea. *J. Geophys. Res.* **95**, 22243–22252.

Bender M. L. and Grande K. D. (1987) Production, respiration, and the isotope geochemistry of O_2 in the upper water column. *Global Biogeochem. Cycles* **1**, 49–59.

Bigeleisen J. and Wolfsberg M. (1958) Theoretical and experimental aspects of isotope effects in chemical kinetics. *Adv. Chem. Phys.* **1**, 15–76.

Blomberg M. R. A. and Siegbahn P. E. M. (2012) Mechanism for N_2O generation in bacterial nitric oxide reductase: a quantum chemical study. *Biochemistry* **51**, 5173–5186.

Brunner B. and Bernasconi S. M. (2005) A revised isotope fractionation model for dissimilatory sulfate reduction in sulfate reducing bacteria. *Geochim. Cosmochim. Acta* **69**, 4759–4771.

Brunner B., Contreras S., Lehmann M. F., Matantseva O., Rollog M., Kalvelage T., Klockgether G., Lavik G., Jetten M. S. M., Kartal B. and Kuypers M. M. M. (2013) Nitrogen isotope effects induced by anammox bacteria. *Proc. Natl. Acad. Sci. USA* **110**, 18994–18999.

Came R. E., Brand U. and Affek H. P. (2014) Clumped isotope signatures in modern brachiopod carbonate. *Chem. Geol.* **377**, 20–30.

Cao X. and Liu Y. (2012) Theoretical estimation of the equilibrium distribution of clumped isotopes in nature. *Geochim. Cosmochim. Acta* **77**, 292–303.

Chakraborty S., Ahmed M., Jackson T. L. and Thiemens M. H. (2008) Experimental test of self-shielding in vacuum ultraviolet photodissociation of CO. *Science* **321**, 1328–1331.

Clog M., Stolper D. and Eiler J. M. (2014) Kinetics of $CO_{2(g)}$–$H_2O_{(l)}$ isotopic exchange, including mass 47 isotopologues. *Chem. Geol.* **395**, 1–10.

Conrad R. and Seiler W. (1979) Field measurements of hydrogen evolution by nitrogen-fixing legumes. *Soil Biol. Biochem.* **11**, 689–690.

Daëron M., Guo W., Eiler J., Genty D., Blamart D., Boch R., Drysdale R., Maire R., Wainer K. and Zanchetta G. (2011) ^{13}C–^{18}O clumping in speleothems: observations from natural caves and precipitation experiments. *Geochim. Cosmochim. Acta* **75**, 3303–3317.

Danielache S. O., Eskebjerg C., Johnson M. S., Ueno Y. and Yoshida N. (2008) High-precision spectroscopy of ^{32}S, ^{33}S, and ^{34}S sulfur dioxide: ultraviolet absorption cross sections and isotope effects. *J. Geophys. Res. Atmos.* **113**, D17314.

Davidson E. A. and Seitzinger S. (2006) The enigma of progress in denitrification research. *Ecol. Appl.* **16**, 2057–2063.

Defliese W. F. and Lohmann K. C. (2015) Non-linear mixing effects on mass-47 CO_2 clumped isotope thermometry: patterns and implications. *Rapid Commun. Mass Spectrom.* **29**, 901–909.

Dennis K. J. and Schrag D. P. (2010) Clumped isotope thermometry of carbonatites as an indicator of diagenetic alteration. *Geochim. Cosmochim. Acta* **74**, 4110–4122.

Dennis K. J., Affek H. P., Passey B. H., Schrag D. P. and Eiler J. M. (2011) Defining an absolute reference frame for 'clumped' isotope studies of CO_2. *Geochim. Cosmochim. Acta* **75**, 7117–7131.

Deutsch C., Sarmiento J. L., Sigman D. M., Gruber N. and Dunne J. P. (2007) Spatial coupling of nitrogen inputs and losses in the ocean. *Nature* **445**, 163–167.

Eagle R. A., Eiler J. M., Tripati A. K., Ries J. B., Freitas P. S., Hiebenthal C., Wanamaker, Jr., A. D., Taviani M., Elliot M., Marenssi S., Nakamura K., Ramirez P. and Roy K. (2013) The influence of temperature and seawater carbonate saturation state on ^{13}C–^{18}O bond ordering in bivalve mollusks. *Biogeosciences* **10**, 4591–4606.

Eagle R. A., Schauble E. A., Tripati A. K., Tütken T., Hulbert R. C. and Eiler J. M. (2010) Body temperatures of modern and extinct species based on ^{13}C–^{18}O bond abundances in apatite. *Proc. Natl. Acad. Sci. USA* **107**, 10377–10382.

Eiler J. M. (2011) Paleoclimate reconstruction using carbonate clumped isotope thermometry. *Quat. Sci. Rev.* **30**, 3575–3588.

Eiler J. M. (2013) The isotopic anomalies of molecules and minerals. *Annu. Rev. Earth Planet. Sci.* **41**, 411–441.

Eiler J. M. and Schauble E. (2004) $^{18}O^{13}C^{16}O$ in the Earth's atmosphere. *Geochim. Cosmochim. Acta* **68**, 4767–4777.

Eiler J. M., Clog M., Magyar P., Piasecki A., Sessions A., Stolper D., Deerberg M., Schlueter H.-J. and Schwieters J. (2013) A high-resolution gas-source isotope ratio mass spectrometer. *Int. J. Mass Spectrom.* **335**, 45–56.

Eisenstadt D., Barkan E., Luz B. and Kaplan A. (2010) Enrichment of oxygen heavy isotopes during photosynthesis in phytoplankton. *Photosynth. Res.* **103**, 97–103.

Eugster O. and Gruber N. (2012) A probabilistic estimate of global marine N-fixation and denitrification. *Global Biogeochem. Cycles* **26**, GB4013.

Eyring H. (1935) The activated complex in chemical reactions. *J. Chem. Phys.* **3**, 107–115.

Farquhar J., Savarino J., Airieau S. and Thiemens M. H. (2001) Observation of wavelength-sensitive mass-independent sulfur isotope effects during SO_2 photolysis: implications for the early atmosphere. *J. Geophys. Res. Planets* **106**, 32829–32839.

Fernandez A., Tang J. and Rosenheim B. E. (2014) Siderite 'clumped' isotope thermometry: a new paleoclimate proxy for humid continental environments. *Geochim. Cosmochim. Acta* **126**, 411–421.

Frame C. H. and Casciotti K. L. (2010) Biogeochemical controls and isotopic signatures of nitrous oxide production by a marine ammonia-oxidizing bacterium. *Biogeosciences* **7**, 2695–2709.

Galloway J. N., Dentener F. J., Capone D. G., Boyer E. W., Howarth R. W., Seitzinger S. P., Asner G. P., Cleveland C. C., Green P. A., Holland E. A., Karl D. M., Michaels A. F., Porter J. H., Townsend A. R. and Vörösmarty C. J. (2004) Nitrogen cycles: past, present, and future. *Biogeochemistry* **70**, 153–226.

Galloway J. N., Townsend A. R., Erisman J. W., Bekunda M., Cai Z., Freney J. R., Martinelli L. A., Seitzinger S. P. and Sutton M. A. (2008) Transformations of the nitrogen cycle: recent trends, questions, and potential solutions. *Science* **320**, 889–892.

Gao Y. Q. and Marcus R. A. (2007) An approximate theory of ozone isotope effects: rate constant ratios and pressure dependence. *J. Chem. Phys.* **127**, 244316.

Ghosh P., Adkins J., Affek H., Balta B., Guo W., Schauble E. A., Schrag D. and Eiler J. M. (2006) ^{13}C–^{18}O bonds in carbonate materials: a new kind of paleothermometer. *Geochim. Cosmochim. Acta* **70**, 1439–1456.

Ghosh P., Eiler J., Campana S. E. and Feeney R. F. (2007) Calibration of the carbonate 'clumped isotope' paleothermometer for otoliths. *Geochim. Cosmochim. Acta* **71**, 2736–2744.

Grosskopf T., Mohr W., Baustian T., Schunck H., Gill D., Kuypers M. M. M., Lavik G., Schmitz R. A., Wallace D. W. R. and LaRoche J. (2012) Doubling of marine dinitrogen-fixation rates based on direct measurements. *Nature* **488**, 361–364.

Gruber N. and Galloway J. N. (2008) An earth-system perspective of the global nitrogen cycle. *Nature* **451**, 293–296.

Guo W., Mosenfelder J. L., Goddard, III, W. A. and Eiler J. M. (2009) Isotopic fractionations associated with phosphoric acid digestion of carbonate minerals: insights from first-principles theoretical modeling and clumped isotope measurements. *Geochim. Cosmochim. Acta* **73**, 7203–7225.

Guy R. D., Fogel M. L. and Berry J. A. (1993) Photosynthetic fractionation of the stable isotopes of oxygen and carbon. *Plant Physiol.* **101**, 37–47.

Hadfield K. L. and Bulen W. A. (1969) Adenosine triphosphate requirement of nitrogenase from Azotobacter vinelandii. *Biochemistry* **8**, 5103–5108.

Hattori S., Danielache S. O., Johnson M. S., Schmidt J. A., Kjaergaard H. G., Toyoda S., Ueno Y. and Yoshida N. (2011) Ultraviolet absorption cross sections of carbonyl sulfide isotopologues $OC^{32}S$, $OC^{33}S$, $OC^{34}S$ and $O^{13}CS$: isotopic fractionation in photolysis and atmospheric implications. *Atmos. Chem. Phys.* **11**, 10293–10303.

Hayes J. M. (2001) Fractionation of carbon and hydrogen isotopes in biosynthetic processes. In *Reviews in Mineralogy and Geochemistry* (eds. J. W. Valley and D. R. Cole). pp. 225–278.

Helman Y., Barkan E., Eisenstadt D., Luz B. and Kaplan A. (2005) Fractionation of the three stable oxygen isotopes by oxygen-producing and oxygen-consuming reactions in photosynthetic organisms. *Plant Physiol.* **138**, 2292–2298.

Henkes G. A., Passey B. H., Wanamaker, Jr., A. D., Grossman E. L., Ambrose, Jr., W. G. and Carroll M. L. (2013) Carbonate clumped isotope compositions of modern marine mollusk and brachiopod shells. *Geochim. Cosmochim. Acta* **106**, 307–325.

Hill P. S., Tripati A. K. and Schauble E. A. (2014) Theoretical constraints on the effects of pH, salinity, and temperature on clumped isotope signatures of dissolved inorganic carbon species and precipitating carbonate minerals. *Geochim. Cosmochim. Acta* **125**, 610–652.

Hillier W. and Wydrzynski T. (2008) ^{18}O–water exchange in photosystem II: substrate binding and intermediates of the water splitting cycle. *Coord. Chem. Rev.* **252**, 306–317.

Hoffman B. M., Lukoyanov D., Yang Z.-Y., Dean D. R. and Seefeldt L. C. (2014) Mechanism of nitrogen fixation by nitrogenase: the next stage. *Chem. Rev.* **114**, 4041–4062.

Jackson E. K., Parshall G. W. and Hardy R. W. F. (1968) Hydrogen reactions of nitrogenase: formation of the molecule HD by nitrogenase and by an inorganic model. *J. Biol. Chem.* **243**, 4952–4958.

Joelsson L. M. T., Forecast R., Schmidt J. A., Meusinger C., Nilsson E. J. K., Ono S. and Johnson M. S. (2014) Relative rate study of the kinetic isotope effect in the $^{13}CH_3D + Cl$ reaction. *Chem. Phys. Lett.* **605–606**, 152–157.

Johnston J. C., Cliff S. S. and Thiemens M. H. (1995) Measurement of multioxygen isotopic ($\delta^{18}O$ and $\delta^{17}O$) fractionation factors in the stratospheric sink reactions of nitrous oxide. *J. Geophys. Res. Atmos.* **100**, 16801–16804.

Jung M.-Y., Well R., Min D., Giesemann A., Park S.-J., Kim J.-G., Kim S.-J. and Rhee S.-K. (2014) Isotopic signatures of N_2O produced by ammonia-oxidizing archaea from soils. *ISME J.* **8**, 1115–1125.

Juranek L. W. and Quay P. D. (2013) Using triple isotopes of dissolved oxygen to evaluate global marine productivity. *Annu. Rev. Mar. Sci.* **5**, 503–524.

Kaiser J. (2011) Technical note: consistent calculation of aquatic gross production from oxygen triple isotope measurements. *Biogeosciences* **8**, 1793–1811.

Kartal B., Maalcke W. J., de Almeida N. M., Cirpus I., Gloerich J., Geerts W., Op den Camp H. J. M., Harhangi H. R., Janssen-Megens E. M., Francoijs K.-J., Stunnenberg H. G., Keltjens J. T., Jetten M. S. M. and Strous M. (2011) Molecular mechanism of anaerobic ammonium oxidation. *Nature* **479**, 127–130.

Kele S., Breitenbach S. F. M., Capezzuoli E., Meckler A. N., Ziegler M., Millan I. M., Kluge T., Deák J., Hanselmann K., John C. M., Yan H., Liu Z. and Bernasconi S. M. (2015) Temperature dependence of oxygen- and clumped isotope fractionation in carbonates: a study of travertines and tufas in the 6–95 °C temperature range. *Geochim. Cosmochim. Acta* **168**, 172–192.

Kluge T. and Affek H. P. (2012) Quantifying kinetic fractionation in bunker cave speleothems using Δ_{47}. *Quat. Sci. Rev.* **49**, 82–94.

Kluge T. and John C. M. (2015a) Effects of brine chemistry and polymorphism on clumped isotopes revealed by laboratory precipitation of mono- and multiphase calcium carbonates. *Geochim. Cosmochim. Acta* **160**, 155–168.

Kluge T. and John C. M. (2015b) Technical note: a simple method for vaterite precipitation for isotopic studies: implications for bulk and clumped isotope analysis. *Biogeosciences* **12**, 3289–3299.

Kluge T., Affek H. P., Dublyansky Y. and Spötl C. (2014a) Devils Hole paleotemperatures and implications for oxygen isotope equilibrium fractionation. *Earth Planet. Sci. Lett.* **400**, 251–260.

Kluge T., Affek H. P., Zhang Y. G., Dublyansky Y., Spötl C., Immenhauser A. and Richter D. K. (2014b) Clumped isotope thermometry of cryogenic cave carbonates. *Geochim. Cosmochim. Acta* **126**, 541–554.

Kluge T., John C. M., Jourdan A.-L., Davis S. and Crawshaw J. (2015) Laboratory calibration of the calcium carbonate clumped isotope thermometer in the 25–250 °C temperature range. *Geochim. Cosmochim. Acta* **157**, 213–227.

Kuypers M. M. M., Lavik G., Woebken D., Schmid M., Fuchs B. M., Amann R., Jørgensen B. B. and Jetten M. S. M. (2005) Massive nitrogen loss from the Benguela upwelling system through anaerobic ammonium oxidation. *Proc. Natl. Acad. Sci. USA* **102**, 6478–6483.

Levine N. M., Bender M. L. and Doney S. C. (2009) The $\delta^{18}O$ of dissolved O_2 as a tracer of mixing and respiration in the mesopelagic ocean. *Global Biogeochem. Cycles* **23**, GB1006.

Lukoyanov D., Yang Z.-Y., Khadka N., Dean D. R., Seefeldt L. C. and Hoffman B. M. (2015) Identification of a key catalytic intermediate demonstrates that nitrogenase is activated by the reversible exchange of N_2 for H_2. *J. Am. Chem. Soc.* **137**, 3610–3615.

Luz B. and Barkan E. (2000) Assessment of oceanic productivity with the triple-isotope composition of dissolved oxygen. *Science* **288**, 2028–2031.

Luz B. and Barkan E. (2011) Proper estimation of marine gross O_2 production with $^{17}O/^{16}O$ and $^{18}O/^{16}O$ ratios of dissolved O_2. *Geophys. Res. Lett.* **38**, L19606.

Lyons J. R. (2007) Mass-independent fractionation of sulfur isotopes by isotope-selective photodissociation of SO_2. *Geophys. Res. Lett.* **34**, L22811.

Mahaffey C., Michaels A. F. and Capone D. G. (2005) The conundrum of marine N_2 fixation. *Am. J. Sci.* **305**, 546–595.

Mathai J. C., Sauna Z. E., John O. and Sitaramam V. (1993) Rate-limiting step in electron transport: osmotically sensitive diffusion of quinones through voids in the bilayer. *J. Biol. Chem.* **268**, 15422–15454.

McEvoy J. P. and Brudvig G. W. (2006) Water-splitting chemistry of photosystem II. *Chem. Rev.* **106**, 4455–4483.

Miller C. E., Onorato R. M., Liang M.-C. and Yung Y. L. (2005) Extraordinary isotopic fractionation in ozone photolysis. *Geophys. Res. Lett.* **32**, L14814.

Moore R. M., Kienast M., Fraser M., Cullen J. J., Deutsch C., Dutkiewicz S., Follows M. J. and Somes C. J. (2014) Extensive hydrogen supersaturations in the western South Atlantic Ocean suggest substantial underestimation of nitrogen fixation. *J. Geophys. Res. Oceans* **119**, 4340–4350.

Moore R. M., Punshon S., Mahaffey C. and Karl D. (2009) The relationship between dissolved hydrogen and nitrogen fixation in ocean waters. *Deep Sea Res. Part I* **56**, 1449–1458.

Mothet A., Sebilo M., Laverman A. M., Vaury V. and Mariotti A. (2013) Is site preference of N_2O a tool to identify benthic denitrifier N_2O? *Environ. Chem.* **10**, 281–284.

Nicholson D., Stanley R. H. R. and Doney S. C. (2014) The triple oxygen isotope tracer of primary productivity in a dynamic ocean model. *Global Biogeochem. Cycles* **28**, 538–552. http://dx.doi.org/10.1002/2013GB004704.

Ono S., Wang D. T., Gruen D. S., Sherwood-Lollar B., Zahniser M. S., McManus B. J. and Nelson D. D. (2014) Measurement of doubly substituted methane isotopologue, $^{13}CH_3D$, by tunable infrared laser direct absorption spectroscopy. *Anal. Chem.* **86**, 6487–6494.

Ono S., Whitehill A. R. and Lyons J. R. (2013) Contribution of isotopologue self-shielding to sulfur mass-independent fractionation during sulfur dioxide photolysis. *J. Geophys. Res. Atmos.* **118**, 2444–2454.

Ostrom N. E., Pitt A., Sutka R., Ostrom P. H., Grandy A. S., Huizinga K. M. and Robertson G. P. (2007) Isotopologue effects during N_2O reduction in soils and in pure cultures and denitrifiers. *J. Geophys. Res.* **112**, G02005.

Passey B. H. and Henkes G. A. (2012) Carbonate clumped isotope bond reordering and geospeedometry. *Earth Planet. Sci. Lett.*, 351–352.

Petrizzo D. A., Young E. D. and Runnegar B. N. (2014) Implications of high-precision measurements of ^{13}C–^{18}O bond ordering in CO_2 for thermometry in modern bivalved mollusc shells. *Geochim. Cosmochim. Acta* **142**, 400–410.

Prokopenko M. G., Hirst M. B., De Brabandere L., Lawrence D. J. P., Berelson W. M., Granger J., Chang B. X., Dawson S., Crane Iii E. J., Chong L., Thamdrup B., Townsend-Small A. and Sigman (2013) Nitrogen losses in anoxic marine sediments driven by Thioploca–anammox bacterial consortia. *Nature* **500**, 194–198.

Quay P. D., Emerson S., Wilbur D. and Stump C. (1993) The $\delta^{18}O$ of dissolved O_2 in the surface waters of the subarctic pacific: a tracer of biological productivity. *J. Geophys. Res.* **98**, 8447–8458.

Rahn T., Zhang H., Wahlen M. and Blake G. A. (1998) Stable isotope fractionation during ultraviolet photolysis of N_2O. *Geophys. Res. Lett.* **25**, 4489–4492.

Rapatskiy L., Cox N., Savitski A., Ames W. M., Sander J., Nowaczyk M. M., Rögner M., Boussac A., Neese F., Messinger J. and Lubitz W. (2012) Detection of the water-binding sites of the oxygen-evolving complex of photosystem II using W-band ^{17}O electron–electron double resonance-detected NMR spectroscopy. *J. Am. Chem. Soc.* **134**, 16619–16634.

Richet P., Bottinga Y. and Javoy M. (1977) A review of hydrogen, carbon, nitrogen, oxygen, sulphur, and chlorine stable isotope fractionation among gaseous molecules. *Annu. Rev. Earth Planet. Sci.* **5**, 65–110.

Riplinger C. and Neese F. (2011) The reaction mechanism of cytochrome P450 NO reductase: a detailed quantum mechanics/molecular mechanics study. *ChemPhysChem* **12**, 3192–3203.

Risgaard-Petersen N., Nielsen L. P., Rysgaard S., Dalsgaard T. and Meyer R. L. (2003) Application of the isotope pairing technique in sediments where anammox and denitrification coexist. *Limnol. Oceanogr. Methods* **1**, 63–73.

Ritchie G. A. F. and Nicholas D. J. D. (1972) Identification of the sources of nitrous oxide produced by oxidative and reductive processes in *Nitrosomonas europaea*. *Biochem. J.* **126**, 1181–1191.

Rohe L., Anderson T.-H., Braker G., Flessa H., Giesemann A., Lewicka-Szczebak D., Wrage-Mönnig N. and Well R. (2014) Dual isotope and isotopomer signatures of nitrous oxide from fungal denitrification – a pure culture study. *Rapid Commun. Mass Spectrom.* **28**, 1893–1903.

Rouvière P. E. and Wolfe R. S. (1988) Novel biochemistry of methanogenesis. *J. Biol. Chem.* **263**, 7913–7916.

Saenger C., Affek H. P., Felis T., Thiagarajan N., Lough J. M. and Holcomb M. (2012) Carbonate clumped isotope variability in shallow water corals: temperature dependence and growth-related vital effects. *Geochim. Cosmochim. Acta* **99**, 224–242.

Santoro A. E., Buchwald C., McIlvin M. R. and Casciotti K. L. (2011) Isotopic signature of N_2O produced by marine ammonia-oxidizing archaea. *Science* **333**, 1282–1285.

Schauble E. A., Ghosh P. and Eiler J. M. (2006) Preferential formation of ^{13}C–^{18}O bonds in carbonate minerals, estimated using first-principles lattice dynamics Geochim. *Cosmochim. Acta* **70**, 2510–2529.

Schmidt J. A. and Johnson M. S. (2015) Clumped isotope perturbation in tropospheric nitrous oxide from stratospheric photolysis. *Geophys. Res. Lett.* **42**, 3546–3552.

Scranton M. I., Novelli P. C., Michaels A., Horrigan S. G. and Carpenter E. J. (1987) Hydrogen production and nitrogen fixation by Oscillatoria thiebautii during in situ incubations1,2. *Limnol. Oceanogr.* **32**, 998–1006.

Seitzinger S., Harrison J. A., Böhlke J. K., Bouwman A. F., Lowrance R., Peterson B., Tobias C. and Van Drecht G. (2006) Denitrification across landscapes and waterscapes: a synthesis. *Ecol. Appl.* **16**, 2064–2090.

Shiro Y., Fujii M., Iizuka T., Adichi S.-I., Tsukamoto K., Nakahara K. and Shoun H. (1995) Spectroscopic and kinetic studies on reaction of cytochrome P450nor with nitric oxide. *J. Biol. Chem.* **270**, 1617–1623.

Shiro Y., Sugimoto H., Tosha T., Nagano S. and Hino T. (2012) Structural basis for nitrous oxide generation by bacterial nitric oxide reductases. *Philos. Trans. R. Soc. B* **367**, 1195–1203.

Stolper D. A., Lawson M., Davis C. L., Ferrira A. A., Santos Neto E. V., Ellis G. S., Lewan M. D., Martini A. M., Tang Y., Schoell M., Sessions A. L. and Eiler J. M. (2014a) Formation temperatures of thermogenic and biogenic methane. *Science* **344**, 1500–1503.

Stolper D. A., Martini A. M., Clog M., Douglas P. M., Shusta S. S., Valentine D. L., Sessions A. L. and Eiler J. M. (2015) Distinguishing and understanding thermogenic and biogenic sources of methane using multiply substituted isotopologues. *Geochim. Cosmochim. Acta* **161**, 219–247.

Stolper D. A., Sessions A. L., Ferreira A. A., Neto E. V. S., Schimmelmann A., Shusta S. S., Valentine D. L. and Eiler J. M. (2014b) Combined ^{13}C–D and D–D clumping in methane: methods and preliminary results. *Geochim. Cosmochim. Acta* **126**, 169–191.

Sutka R. L., Adams G. C., Ostrom N. E. and Ostrom P. H. (2008) Isotopologue fractionation during N_2O production by fungal denitrification. *Rapid Commun. Mass Spectrom.* **22**.

Sutka R. L., Ostrom N. E., Ostrom P. H., Gandhi H. and Breznak J. A. (2003) Nitrogen isotopomer site preference of N_2O produced by *Nitrosomonas europaea* and *Methylococcus capsulatus* Bath. *Rapid Commun. Mass Spectrom.* **17**, 728–745.

Tang J., Dietzel M., Fernandez A., Tripati A. K. and Rosenheim B. E. (2014) Evaluation of kinetic effects on clumped isotope fractionation (Δ_{47}) during inorganic calcite precipitation. *Geochim. Cosmochim. Acta* **134**, 120–136.

Thiagarajan N., Adkins J. and Eiler J. (2011) Carbonate clumped isotope thermometry of deep-sea corals and implications for vital effects. *Geochim. Cosmochim. Acta* **75**, 4416–4425.

Toyoda S., Mutobe H., Yamagishi H., Yoshida N. and Tanji Y. (2005) Fractionation of N_2O isotopomers during production by denitrifier. *Soil Biol. Biochem.* **37**, 1535–1545.

Tripati A. K., Eagle R. A., Thiagarajan N., Gagnon A. C., Bauch H., Halloran P. R. and Eiler J. M. (2010) Apparent equilibrium ^{13}C–^{18}O isotope signatures and 'clumped isotope' thermometry in foraminifera and coccoliths. *Geochim. Cosmochim. Acta* **74**, 5697–5717.

Valentine D. L., Chidthaisong A., Rice A., Reeburgh W. S. and Tyler S. C. (2004) Carbon and hydrogen isotope fractionation by moderately thermophilic methanogens1. *Geochim. Cosmochim. Acta* **68**, 1571–1590.

Vignais P. M. (2005) H/D exchange reactions and mechanistic aspects of the hydrogenases. *Coord. Chem. Rev.* **249**, 1677–1690.

Wang D. T., Gruen D. S., Lollar B. S., Hinrichs K.-U., Stewart L. C., Holden J. F., Hristov A. N., Pohlman J. W., Morrill P. L., Könneke M., Delwiche K. B., Reeves E. P., Sutcliffe C. N., Ritter D. J., Seewald J. S., McIntosh J. C., Hemond H. F., Kubo M. D., Cardace D., Hoehler T. M. and Ono S. (2015) Nonequilibrium clumped isotope signals in microbial methane. *Science* **348**, 428–431.

Wang Z., Schauble E. A. and Eiler J. M. (2004) Equilibrium thermodynamics of multiply substituted isotopologues of molecular gases. *Geochim. Cosmochim. Acta* **68**, 4779–4797.

Webb M. A. and Miller T. F. (2014) Position-specific and clumped stable isotope studies: comparison of the urey and path-integral approaches for carbon dioxide, nitrous oxide, methane, and propane. *J. Phys. Chem. A* **118**, 467–474.

Whitehill A. R., Xie C., Hu X., Xie D., Guo H. and Ono S. (2013) Vibronic origin of sulfur mass-independent isotope effect in photoexcitation of SO_2 and the implications to the early earth's atmosphere. *Proc. Natl. Acad. Sci. USA* **110**, 17697–17702.

Whiticar M. J., Faber E. and Schoell M. (1986) Biogenic methane formation in marine and freshwater environments: CO_2 reduction vs. acetate fermentation—isotope evidence. *Geochim. Cosmochim. Acta* **50**, 693–709.

Wilson S. T., del Valle D. A., Robidart J. C., Zehr J. P. and Karl D. M. (2013) Dissolved hydrogen and nitrogen fixation in the oligotrophic North Pacific Subtropical Gyre. *Environ. Microbiol. Rep.* **5**, 697–704.

Yamazaki T., Hozuki T., Arai K., Toyoda S., Koba K., Fujiwara T. and Yoshida N. (2014) Isotopomeric characterization of nitrous oxide produced by reaction of enzymes extracted from nitrifying and denitrifying bacteria. *Biogeosciences* **11**, 2679–2689.

Yang H., Gandhi H., Ostrom N. E. and Hegg E. L. (2014) Isotopic Fractionation by a fungal P450 nitric oxide reductase during the production of N_2O. *Environ. Sci. Technol.* **48**, 10707–10715.

Yang H., Gandhi H., Shi L., Kreuzer H. W., Ostrom N. E. and Hegg E. L. (2012) Using gas chromatography/isotope ratio mass spectrometry to determine the fractionation factor for H_2 production by hydrogenases. *Rapid Commun. Mass Spectrom.* **26**, 61–68.

Yang Z.-Y., Khadka N., Lukoyanov D., Hoffman B. M., Dean D. R. and Seefeldt L. C. (2013) On reversible H_2 loss upon N_2 binding to FeMo-cofactor of nitrogenase. *Proc. Natl. Acad. Sci. USA* **110**, 16327–16332.

Yeung L. Y., Affek H. P., Hoag K. J., Guo W., Wiegel A. A., Atlas E. L., Schauffler S. M., Okumura M., Boering K. A. and Eiler J. M. (2009) Large and unexpected enrichment in stratospheric $^{16}O^{13}C^{18}O$ and its meridional variation. *Proc. Natl. Acad. Sci. USA* **106**, 11496–11501.

Yeung L. Y., Ash J. L. and Young E. D. (2014) Rapid photochemical equilibration of isotope bond ordering in O_2. *J. Geophys. Res.* **119**, 10552–10566.

Yeung L. Y., Ash J. L. and Young E. D. (2015) Biological signatures in clumped isotopes of O_2. *Science* **348**, 431–434.

Yeung L. Y., Young E. D. and Schauble E. A. (2012) Measurements of $^{18}O^{18}O$ and $^{17}O^{18}O$ in the atmosphere and the influence of isotope-exchange reactions. *J. Geophys. Res.* **117**, D18306.

Young E. D., Galy A. and Nagahara H. (2002) Kinetic and equilibrium mass-dependent isotope fractionation laws in nature and their geochemical and cosmochemical significance. *Geochim. Cosmochim. Acta* **66**, 1095–1104.

Young E., Rumble D., Freedman P., Schauble E. and Guo W. (2011) Invited: high mass resolution gas-source mass spectrometry. *Mineral. Mag.* **73**, 2229.

Zaarur S., Affek H. P. and Brandon M. T. (2013) A revised calibration of the clumped isotope thermometer. *Earth Planet. Sci. Lett.* **382**, 47–57.

Associate editor: F. McDermott